--- Chapter 4 ---

Electrophysiological characterization of Grueneberg ganglion olfactory neurons: chemosensory responses

Cambrian Y. Liu, Cheng Xiao, Scott E. Fraser, Henry A. Lester, David S. Koos

D.S.K. assisted in the generation of the data and images shown in Figure 9.

ABSTRACT

This study provides an electrophysiological characterization of chemosensory function in Grueneberg ganglion (GG) olfactory neurons in an acute slice preparation of the mouse nasal vestibule. In patch clamp recordings, two established rodent pheromones, 2,5-dimethylpyrazine (2,5-DMP) and 2-heptanone, had excitatory and inhibitory effects, respectively, on the spontaneous firing of GG neurons. The pheromones affected all 3 patterns of spontaneous discharge. GG neurons were excited by 8-br-cGMP and the phosphodiesterase inhibitor IBMX. While responses to 8-br-cGMP and IBMX depended on the expression of the cyclic nucleotide gated cationic channel subunit CNGA3, responses to 2,5-DMP were still present in *Cnga3*$^{-/-}$ mice. Immunohistochemical and extravasation experiments demonstrated that GG neurons reside near a vascular bed. The spontaneous firing rate of GG neurons was reduced by exposure to serum and cortisol. These results indicate that GG neurons encode chemosensory information as bidirectional changes in firing rate and suggest a role for serum modulation of olfactory activity.

KEYWORDS

Patch clamp, 2,5-dimethylpyrazine, 2-heptanone, CNGA3, cGMP, odorant inhibition, pheromones, vasculature, Evans blue, extravasation, serum, cortisol

INTRODUCTION

The Grueneberg ganglion (GG) is a primary mammalian olfactory subsystem that is composed of ~1,000 glial-wrapped neuronal cell bodies located on both sides of the cartilaginous septum in the far-rostral nasal vestibule. Whereas olfactory sensory neurons (OSNs) in the main olfactory epithelium (MOE) are arranged to form a pseudostratified epithelium, GG neurons form discrete clusters that collectively occupy an arrowhead-shaped domain in the nasal vestibule. Mouse GG neurons express olfactory marker protein (OMP), a specific marker of mature primary OSNs, and possess axons that collect to form 8-12 glomeruli in the necklace-like domain of the olfactory bulb (Fleischer et al. 2006; Fuss et al. 2005; Grüneberg 1973; Koos and Fraser 2005; Roppolo et al. 2006; Storan and Key 2006).

Functionally, GG neurons *in vivo* homogeneously exhibit increased c-Fos expresion when exposed to the pheromones 2,5-dimethylpyrazine (2,5-DMP) and 2,3-dimethylpyrazine (2,3-DMP), but not to 2-heptanone (Mamasuew et al. 2011a). Both 2,5-DMP and 2-heptanone have been shown to perturb the reproductive physiology of rodents and are secreted in urine in an adrenal-mediated manner (Novotny et al. 1986). These pheromones stimulated OSNs and necklace glomeruli, in the absence of the main olfactory cAMP-gated channel subunit CNGA2 (Lin et al. 2004), as well as vomeronasal sensory neurons (VSNs) of the vomeronasal organ (VNO) (Leinders-Zufall et al. 2000; Riviere et al. 2009). In the GG, the c-Fos response to DMP compounds *in vivo* depended on the cGMP-gated cationic channel subunit CNGA3 and the membrane-bound receptor guanylate cyclase pGC-G (Mamasuew et al. 2011b), both critical components of a unique cGMP transduction pathway in the GG (Fleischer et al. 2009; Liu et al. 2009).

A second chemosensory modality for the GG involves the detection of putative alarm pheromones. Mouse GG neurons homogeneously exhibit cytosolic [Ca^{2+}] bursts in direct response to an unknown water-soluble compound collected during the asphyxiation of mice. Moreover, this compound induced freezing behavior in mice that was abolished by axotomy of the GG (Brechbuhl et al. 2008).

GG neurons act as finely-tuned cold sensors. Decreasing the ambient temperature from 25˚ C to 15˚ C resulted in increased c-Fos expression in the GG neurons of neonatal mice, an effect that was

CNGA3-dependent (Mamasuew et al. 2008; Mamasuew et al. 2010). GG neurons homogeneously exhibit [Ca^{2+}] bursts in response to cold in a temperature-dependent manner, with an ET_{50} of ~16˚ C. However, *in vitro* thermosensitivity of the GG was not reliant on CNGA3 (Schmid et al. 2010).

We recently reported an acute slice preparation that enabled patch clamp recordings of the GG (Chapter 3). GG neurons are functionally heterogeneous in that different neurons spontaneously discharge in different patterns that do not readily interconvert. These patterns could be broadly characterized as repetitive single-spike (RSS), phasic, or sporadic. Here, we describe the electrophysiological responses of GG neurons to 2,5-DMP, 2-heptanone, general odorants, and mouse serum.

MATERIALS AND METHODS

Animals

Mice were maintained as per Caltech-approved protocol. The characterization of OMP-GFP mice has been described previously (Potter et al. 2001). *Cnga3*$^{-/-}$ mice were a gift from B. Chang. These mice were maintained in the Jackson Laboratory in the Eye Mutant Resource as the cone photoreceptor function loss (cpfl5) mouse line. Genetic analysis of these mice showed that they carried a naturally-occurring point mutation in position 492 (A→G) in exon 5 of the *Cnga3* cDNA. This resulted in a T164A missense mutation in the CNGA3 protein product. Cpfl5 mice did not exhibit any cone electroretinography function (B. Chang, personal correspondence).

OMP-GFP mice were on a BL/6/129 background. *Cnga3*$^{-/-}$ and *Cnga3*$^{+/-}$ mice were on RHJ/LeJ (JR 5415) background. All animals used were postnatal.

Genotyping

The point mutation in *Cnga3*$^{-/-}$ mice was detected in genotyping assays from tail genomic DNA prepared using the PureGene kit (Qiagen). A segment of the *Cnga3* gene was amplified with PCR using HotStar Taq (Qiagen) with the following primer sequences (5’ to 3’): CTTGGACTAGTCTGCAGATG (forward) and TGGACCAGTCAAGTCCGTGG (reverse). Because the point mutation in *Cnga3* created a

restriction site, PCR products were digested with the restriction enzyme SmaI. Digestion products were resolved on a 4.5% NuSieve 3-1 agarose (Lonza) gel prepared in Tris/borate/EDTA (TBE) buffer. Tails from *Cnga3*$^{+/+}$ mice analyzed in this manner would yield one band of 90 bp; from *Cnga*$^{-/-}$ mice, 2 bands of 53 and 37 bp; from *Cnga3*$^{+/-}$ mice, 3 bands of 90, 53, and 37 bp.

Electrophysiology

Using the previously described protocol (Chapter 3), electrophysiological recordings were performed using acute nasal vestibule slices that were prepared from OMP-GFP$^{+/-}$ (mixed C57BL/6 x 129 background) or *Cnga3*$^{+/-}$ / *Cnga3*$^{-/-}$ mice in the age range of p0 to p13. Briefly, mice were euthanized and decapitated. The nasal vestibule was removed and sliced, while immersed in ice-cold modified glycerol HEPES-buffered saline (gHBS), in the transverse plane to a thickness of 100 µm with a vibratome (VT-1000S, Leica). Nasal vestibule slices were washed with HEPES-buffered saline (HBS) at room temperature and incubated with 0.1% type-II collagenase (Invitrogen)-HBS at 37˚C for 10 min. Slices were twice washed with warmed HBS. For cell-attached recordings, nasal vestibule slices were recovered in HBS at 37˚C for 5 min; for whole-cell recordings, the slices were recovered in the same manner, but for 25 min. Tissue was returned to room temperature for >30 min prior to recording. Recipe for gHBS was (in mM): 272 glycerol, 2.5 KCl, 10 HEPES, 10 D-glucose, 2 $CaCl_2$, 1.3 $MgCl_2$, pH 7.4. Recipe for HBS was (in mM): 142 NaCl, 2.5 KCl, 10 HEPES, 10 D-glucose, 2 $CaCl_2$, 1.3 $MgCl_2$, pH 7.4, osmolarity 280-290 mOsm/kg. Recipe for nominal Ca^{2+}-free HBS used in some experiments was (in mM): 142 NaCl, 2.5 KCl, 10 HEPES, 10 D-glucose, 3.3 $MgCl_2$, 0.5 EGTA, pH 7.4, osmolarity 280-290 mOsm/kg.

Neurons were visualized on an upright microscope (BX50WI, Olympus) with brightfield and fluorescent illumination. Tissue slices were kept under HBS delivered from a continuous gravity-based perfusion system. GG neurons could be identified in OMP-GFP mice by their GFP fluorescence. For recordings from nonfluorescing GG neurons (*i.e.*, *Cnga3*-mutant mice and wild-type mice), the neurons were identified by their large diameter, protrusion at the surface of the tissue slice, clustered arrangement, stereotyped location relative to blood vessels and nonsensory epithelium, and exhibition of spontaneous

firing and/or fast-inactivating voltage-gated Na^+ channels. Electrical activity was recorded with MultiClamp 700B amplifiers (Axon Instruments, Molecular Devices), Digidata 1200 analog-to-digital converters (Axon Instruments), and pCLAMP 9.2 software (Axon Instruments). Data were sampled at 10 kHz and filtered at 2 kHz. The junction potential between patch pipette and bath solution was nulled immediately before applying suction to the cell membrane.

For extracellular cell-attached recordings, the patch pipettes were filled with the bath solution (usually HBS or HBS supplemented with diluent (*e.g.*, DMSO)). For whole-cell recordings, to characterize intrinsic membrane properties such as resting membrane potential (V_m), Na^+ current activation, and I_h, the patch pipettes were filled with a high-Cl^-, K^+-based intrapipette solution containing (in mM): 140 KCl, 10 HEPES, 1 $CaCl_2$, 2 $MgCl_2$, 2 K_2ATP, 5 EGTA, pH 7.4, osmolarity 290 mOsm/kg. The predicted junction potential for this intrapipette solution with the HBS bath was 4.1 mV. To study odorant-evoked and pharmacologically modified currents, patch piettes were filled with a high-Cl^-, low Ca^{2+} intrapipette solution containing (in mM): 90 KCl, 50 K-gluconate, 10 HEPES, 5 $MgCl_2$, 5 K_2ATP, 1 Na_3GTP, 0.1 EGTA, pH 7.4, osmolarity 290 mOsm/kg. Predicted junction potential for this intra-pipette solution with the HBS bath was 8.5 mV. Junction potentials were corrected offline. Patch pipettes used for cell-attached recordings had resistances of 2-5 MΩ; those used for whole-cell recordings had resistances of 4-8 MΩ.

In cell-attached recordings, spontaneous firing of GG neurons was recorded in current-clamp mode with 0 pA holding current, to minimize artifacts resulting from holding current over the patch. In whole-cell recordings, we periodically monitored the membrane capacitance and the series resistance over the recording; otherwise, we neither cancelled the capacitive transients nor compensated the series resistance. Data were discarded if the series resistance exceeded 30 MΩ.

Working solutions of odorants and pharmacological compounds-of-interest were freshly prepared on the day of the experiment. Unless otherwise indicated, all chemicals were purchased from Sigma. Liquids were normally diluted 1:1,000, 1:5,000, 1:10,000, etc. to give the reported concentrations. Thapsigargin was purchased from Tocris Bioscience and diluted to a stock concentration of 20 mM in

DMSO. IBMX was diluted to a stock concentration of 0.5 M in DMSO. Cortisol was diluted to a stock concentration of 100 mM in DMSO. Responses were tested by filling a glass pipette with a 2 μm diameter tip with the compound of interest diluted in the bath solution (usually HBS). This "puff" pipette was mounted on a piezoelectric manipulator and connected to a controlled pressure source (Parker Instrumentation). The puff pipette was placed 5-20 μm from the cell soma. Odorants and compounds of interest were applied to the cell by computer-controlled pressure pulses (10 psi, variable durations). We did not test compounds at concentrations of >15 mM due to the potential for nonspecific artifacts relating to sudden changes in osmolarity.

Immunohistochemistry

Immunohistochemistry was performed as described previously (Liu et al. 2009). Primary antibodies used were rat anti-CD31 (1:100, BD Biosciences, cat# 557355), rabbit anti-LYVE1 (1:500, Abcam, cat# ab14917), rabbit anti-vWF (1:800, Abcam, cat# ab6994), rabbit anti-αSMA (1:500, Abcam, cat# ab5694), rabbit anti-DβH (1:500, Abcam, cat# ab43868) and rat anti-PV-1 (1:40, MECA-32 clone, BD Biosciences, cat# 550563). Secondary antibodies used were biotinylated mouse-adsorbed rabbit anti-rat IgG (3 μg/mL, Vector Labs), biotinylated goat anti-rabbit IgG (3 μg/mL, Vector Labs), and Alexa Fluor 555-conjugated donkey anti-rabbit IgG (4 μg/mL, Invitrogen). Tertiary labels used were peroxidase-streptavidin (2.5 μg/mL, MP Bio), Alexa Fluor 555-conjugated steptavidin (2 μg/mL, Invitrogen), and Alexa Fluor 633-conjugated streptavidin (2 μg/mL, Invitrogen).

For PV-1 staining, freshly dissected nasal vestibules were embedded in Tissue-Tek O.C.T. (Sakura) and flash-frozen in liquid nitrogen. Sections of 12 μm thickness were prepared on a freezing microtome and mounted onto Superfrost Plus (Fisherbrand) slides. Slides were immersed in acetone at -20˚C for 15 min. Sections were washed with phosphate-buffered saline (PBS) and incubated with the PV-1 antibody in PBS. Stain was developed with a heavy-metal enhanced diaminobenzidine-peroxide kit (Thermo Scientific), as performed previously (Liu et al. 2009).

All other antibodies were applied to 12-18 μm cryosections that had been prepared from tissue fixed in 4% (w/v) paraformaldehyde-PBS. Triton-X was omitted from some of the staining solutions to optimize membrane labelin; otherwise, it was used at 0.3%. All slides were mounted with Fluoro-Gel (Electron Microscopy Sciences) and coverslipped prior to imaging.

Extravasation assays

Intraperitoneal injections of 500 μL 2% Evans blue (EB)/PBS were performed on adult mice (ages: 1.5-2 months). After 60 min, mice were anesthetized with intraperitoneal injections of 0.5-0.7 mL of 20 mg/mL 2,2,2-tribromoethanol/PBS. Mice were transcardially exsanguinated with 1 U/mL heparin/PBS and then fixed with 4% w/v paraformaldehyde/PBS. Perfusion solutions were delivered with a variable-flow peristaltic pump through an aortic puncture. The nasal cavities and olfactory bulbs of transcardially perfused mice were isolated and immersed in 4% paraformaldehyde overnight at 4˚C.

Nasal cavities and brains were bisected for gross examination on widefield light microscopes. The MOE and VNO were decalcified overnight in 14% w/v EDTA/water. Tissues were cryoprotected in an ascending sucrose/PBS series (10%, 20%, 30%), embedded in Tissue-Tek O.C.T. (Sakura), and sectioned to 18 μm thickness on a freezing microtome. Sections were immediately adhered to slides, defrosted, and imaged (without coverslipping) on confocal microscopes.

To verify EB-labeling of olfactory subsystems, we directly applied EB to the nasal cavity. Adult mice (age: 1.5-2 months) were anesthetized with intraperitoneal injections of 20 mg/mL 2,2,2-tribromoethanol/PBS. A narrow gel-loading tip containing 5 uL of 2% EB/PBS solution was partially inserted into the left nasal cavity. After ejection of dye, the tip was removed. Mice remained anesthetized for 30 min prior to euthanasia and cardiac perfusion as described above. To remove excess dye, nasal cavities were washed with several changes of PBS before overnight immersion in cold 4% paraformaldehyde/PBS. Histological examination of specimens was performed as described above.

Isolation of serum

To isolate mouse serum, 3 wild-type BL/6/129 mice (p10) were separated from the litter and moved in a cardboard box to a separate dissection station away from the animal housing facility. Mice were immediately euthanized and decapitated over a 60-mm Petri dish containing 2 mL HBS. Blood was drained from the head and body cavities into the dish, with care to avoid contamination with urine and fecal matter. An additional 4 mL of HBS was added to the dish. Dish contents were triturated prior to centrifugation at 10,000 rpm at room temperature for 3 min. The supernatant was immediately frozen and stored at -80˚C. Serum isolate and electrophysiological bath solutions were matched in osmolarity by adjusting [NaCl]. Prior to testing, serum was passed through a 0.22-µm filter.

Imaging

Fluorescent images were obtained from a Zeiss LSM510 upright confocal microscope with laser excitation wavelengths of 488 nm, 543 nm, and 633 nm. The pinhole diameter was varied to obtain optical sections of various thicknesses. Image stacks were projected at maximum intensity. For the analysis of Evans blue (EB) extravasation, we took advantage of the far-red fluorescence of EB (Saria and Lundberg 1983) and excited tissue samples with the 633-nm laser. The images of the nasal vestibule, MOE, VNO, and olfactory bulb were obtained in succession and at the same laser power and photomultiplier gain. Brightfield photomicrographs were snapped on a Zeiss upright Axioplan microscope.

Data analysis

Electrophysiological recordings were analyzed in Clampfit 9.2 and in MATLAB 7.4.0 with custom-written routines. Recordings contained precise information about the onset and duration of the pressure puff. Action potentials (APs) were collection using the template search feature in Clampfit. The time-of-peak values of neighboring APs were used to calculate plots of instantaneous frequency vs. time. Desensitizing excitatory responses were fit over the duration of the puff to the following functional form:

$$f(t) = A\left(1 - e^{-t/\tau_a}\right)e^{-t/\tau_{ds}} + C$$

where *f(t)* represents the instantaneous frequency *f* (in Hz) as a function of time *t* (in s), τ_a and τ_{ds} represent the exponential time constants of activation and desensitization, respectively, and *A* and *C* are constants. The value of C was affixed to the average initial firing frequency (measured over 5-60 s) in RSS-firing and sporadic-firing neurons; in phasic-firing neurons, it was affixed to the average initial intraburst frequency. For excitatory responses, the fits were applied to the instantaneous intraburst frequencies in phasic-firing neurons, the total instantaneous frequency in RSS-firing neurons, and a 1-2 s bin of the total firing frequency in sporadic-firing neurons. The maximum value of *f(t)*, divided by *C*, provided an estimate of the response magnitude. Values of τ_a, τ_{ds}, and A were provided by fitting functions in MATLAB. Non-desensitizing excitatory activating responses during the puff were fit to the form:

$$f(t) = A\left(1 - e^{-t/\tau_a}\right) + C$$

where the variables have their usual meanings and constraints. The decay of the excitatory response after puff termination was fit to the function:

$$f(t) = Ae^{-t/\tau_{de}} + C$$

where τ_{de} represents the exponential time constant of decay. *C* was affixed to be the average instantaneous frequency in a time window (1-5 s) prior to puff termination. These functions were also applied to the analysis of ligand-induced inward and outward currents in whole-cell recordings, when appropriate (*i.e.*, when they provided good fits to the data).

Small inhibitory responses (change in firing rate $\Delta f < 25\%$) could be fit to the described functions. However, larger inhibitory responses were associated with the loss of spikes (*i.e.*, sampling resolution); these responses were quantified by comparing the total spike frequency during the puff to the spike frequency in the 5-60 s before the puff. A total lack of spikes during the puff was considered 100% inhibition ($\Delta f = -100\%$). A doubling of the firing rate was considered $\Delta f = +100\%$. For both excitatory and inhibitory responses, irreversible changes were considered a sign of cell death or seal loss. Data from

these neurons were not included in the analyses. In the reporting of effects, the given error is the inferential or standard error of the mean; the age range of the tested mice is also included.

Data were pooled from multiple neurons to derive dose-response relationships. In the analysis of responses to 2,5-DMP and 2,3-DMP, the responses did not exhibit a Gaussian distribution due to a significant fraction of non-responders. Population response magnitudes for 2,5-DMP and 2,3-DMP were thus calculated as probabilistic expected responses:

$$E(r_i) = n_i \bar{r}_i$$

where $\bar{r}_i$ indicates the average response magnitude among responding neurons at concentration *i*, n_i is the fraction of the tested neurons that responded at concentration *i*, and $E(r_i)$ represents the expected response magnitude for the population. The collection of $E(r_i)$ were used to calculate the dose-response relationship. In the analysis of 2-heptanone, the average inhibitory response over all tested neurons at a given concentration was used to compute the dose-response curve. This curve was fit to a Hill equation:

$$r(i) = \frac{i^a}{i^a + i_{50}}$$

where $r(i)$ is the response at concentration *i*, *a* is the Hill coefficient, and i_{50} is the half-inhibitory concentration (IC_{50}).

Fluorescent images were analyzed in ImageJ (NIH). All adjustments to image contrast and brightness were uniform and linear.

RESULTS

GG neurons in acute slices of the mouse nasal vestibule were exposed to 10 psi pressure ejections of various durations ("puffs"). The puffs were delivered from a micropipette that was placed ~20 µm from the cell soma (Fig. 1A). The micropipette contained the odorants/drugs that were diluted in the extracellular solution to the reported concentrations. The effect of the puff on the spontaneous firing of the neuron was recorded in the extracellular loose-seal configuration. The frequency vs. time plot in Fig. 1B demonstrates the effect of a 10 s puff of odorant-free saline on the spontaneous firing of one neuron.

Overall, these puffs induced no change (Δf: -0.3 ± 1.4%, n=8, p7) in the firing rate or pattern of the neurons.

Responses to 2,5-DMP and 2,3-DMP

We examined the effects of 20 s puffs of 2,5-DMP on the spontaneous firing of GG neurons. Excitatory responses to 9.3 mM 2,5-DMP were found in 33/45 (73%) neurons. Fig. 2 shows the effects of 2,5-DMP on the intrinsic patterns of spontaneous discharge. In phasic-firing neurons, the responses appeared as transient elevations in the intraburst frequency (Fig. 2A). In RSS-firing neurons (Fig. 2B), the total firing rate was transiently elevated by 2,5-DMP. In sporadic-firing neurons, the frequency vs. time plot in Fig. 2C indicates a transient burst of high-frequency spikes.

Fig. 3A shows the composite time dependence of the changes in instantaneous firing frequency induced by 20 s puffs of 1.9-9.3 mM 2,5-DMP. There was no visible latency to the responses at a maximum sampling frequency of 25 Hz. The responses were >90% desensitized by the end of the 20 s puff. The time dependence of the responses could be fit by an inactivating exponential function, which yielded a median activation time constant (τ_a) of 0.89 s and a median desensitization time constant (τ_{ds}) of 4.4 s (n=39).

GG responses to 2,5-DMP were dose- and age-dependent. Fig. 3B shows the response magnitude at 3 different concentrations (9.3, 4.6, 1.9 mM) of 2,5-DMP. The responses decreased with decreasing concentration of 2,5-DMP. Fig. 4B indicates that when GG neurons from p0-p5 mice were puffed with 9.3 mM 2,5-DMP, the responses tended to be most robust at p0-p1, when 20/21 neurons were vigorously excited. In contrast, in p3-p4 mice, only 7/15 GG neurons were excited by 2,5-DMP, and these neurons were weakly affected.

Similar to 2,5-DMP, 20 s puffs of 9.3 mM 2,3-DMP induced elevations in repetitive firing rate in 5/5 GG neurons from p1 mice (Supplementary Fig. 1). Responses to 1.9-9.3 mM 2,3-DMP had no latency, with median τ_a equal to 0.66 s and median τ_{ds} equal to 8.3 s (n=14). These parameters did not differ significantly between 2,5-DMP and 2,3-DMP (p values: τ_a= 0.27, τ_{ds} = 0.25, t-test). The effects of

2,3-DMP were dose-dependent (Fig. 3D) and declined with age (Δf, p7 = 11 ± 1%, n=5; Δf, p2 = 77 ± 20%, n=5).

We tested the effect of a related molecule, pyrazine, on GG neurons. 20 s puffs of 10 mM pyrazine excited 0/10 GG neurons from a p2 mouse. In the same mouse, 6/9 GG neurons were excited by 20 s puffs of 9.3 mM 2,5-DMP. Thus, GG neurons selectively detect 2,5-DMP and 2,3-DMP.

Responses to general odorant exposure

We tested whether 2-heptanone, a known activator of the necklace glomeruli (Lin et al. 2004), could alter spontaneous activity in the GG. In extracellular loose-seal recordings, pressure ejections (5-20 s duration) of 1.4-14 mM 2-heptanone resulted in the reversible reduction of the total spontaneous firing rate in 26/26 GG neurons from p0-p4 mice. Fig. 4A shows the inhibition of firing induced by a 5 s puff of 3.6 mM 2-heptanone. This inhibitory response is evident in the frequency vs. time plot of Fig. 4B. The inhibitory effect of 2-heptanone was dose dependent, exhibiting an IC_{50} of ~2 mM and a Hill coefficient of ~1.5 (Fig. 4C). When 7.2 mM 2-heptanone was superfused onto GG neurons, the inhibitory effect persisted for the duration (~5 min) of the exposure (n=5). Responses to 2-heptanone were still present when neurons were pretreated with 20 μM thapsigargin for 30 min (n=5) (Supplementary Fig. 2).

In whole-cell recordings, 20 s puffs of 7.2 mM 2-heptanone elicited an outward current from a holding potential of -64 mV in 5/5 examined GG neurons. These currents had peak amplitudes of 2.2 ± 0.6 pA/pF and an exponential rise time of 7.2 ± 1.9 s. There was no visible desensitization of currents during 20 s puffs. Fig. 4D shows that the currents increased in magnitude at more-positive holding potentials. In current-clamp recordings, 7.2 mM 2-heptanone induced a reversible hyperpolarization of the resting potential (Fig. 4E).

The inhibition of spontaneous firing was not specific to 2-heptanone. We tested, with 20 s puffs, the effects of 2-heptanol (alcohol), ethanol (alcohol), eucalyptol (ether), isovaleric acid (carboxylic acid), citral (aldehyde), and dimethylsulfoxide (sulfur) in the range of 5-10 mM. Table 1 lists the inhibitory responses induced by each of these tested odorants. There were some differences in the sensitivity of GG

neurons to these various substances. For example, at 150 μM, outside of the detection range for 2-heptanone, GG neurons responded to 2-heptanol with a 26 ± 13% reduction in total firing rate (n=3). In contrast, at 8.6 mM, at which GG neurons exhibit >85% inhibition due to 2-heptanone and 2-heptanol, ethanol inhibited only an 18 ± 9% inhibition. In whole-cell recordings, the effects of eucalyptol on membrane currents were similar to those observed with 2-heptanone (Supplementary Fig. 4).

Re-examining the puffs of 2,5-DMP, 2,3-DMP, and pyrazine, we found that the excitatory responses could be accompanied by inhibitory ones in the same cell. For example, at the tail of the response shown in Fig. 2B, when the excitatory response was fully desensitized, an underlying inhibitory response is apparent. Thus, the specific excitatory responses to DMP isoforms can occur against a background of nonspecific odorant-elicited inhibition. The inhibitory responses were not due to sudden changes in osmolarity, as puffs of 10 mM D-glucose altered neither firing rate nor pattern.

Function of the cGMP signaling pathway

GG neurons are proposed to employ a unique cGMP transduction pathway for chemosensory and thermosensory function (Mamasuew et al. 2011b; Mamasuew et al. 2010). Consistent with this proposal, GG neurons are excited by exposure to 8-br-cGMP, a membrane-permeant cGMP analog. 20 s puffs of 1.3 mM 8-br-cGMP excited 11/12 GG neurons (Δf: 130 ± 41%, p4-p6) (Fig. 5A). In RSS-firing and sporadic-firing neurons, the responses appeared as increases in the total firing frequency (Fig. 5B). In phasic-firing neurons, the responses were characterized by an increase in the intraburst firing frequency. The firing rates rose with a single-exponential τ_a equal to 10 ± 3.4 s during a 20 s puff and decayed with τ_{de} equal to 63 ± 9.3 s following puff termination.

We compared the responses to 8-br-cGMP with those elicited by 20 s puffs of 3-isobutyl-1-methylxanthine (IBMX), an inhibitor of phosphodiesterase proteins. In total, 20/20 GG neurons from p2-p6 mice responded to 100 μM IBMX. In 11/20 neurons, IBMX increased the total firing frequency during the puff (Fig. 5C). In the other 9 responsive neurons, the total firing frequency was decreased. As Fig. 5D illustrates, in these neurons, puff onset resulted in a burst of high-frequency, small-magnitude spikes,

followed by the sustained inhibition. These observations suggest that IBMX causes a strong depolarization of the membrane potential, which can inhibit repetitive firing in some neurons (Chapter 3). The decay time constant (τ_{de}: 6.7 ± 2.0 s, n=14) was smaller for IBMX responses (p = 0.0003) than for 8-br-cGMP responses.

In whole-cell recordings, at a holding potential of -64 mV, a 20 s puff of 100 μM IBMX elicited inward currents in 13/14 (93%) GG neurons. Fig. 6A illustrates that these currents peaked at 2.5 ± 0.6 s and had a peak amplitude -4.3 ± 0.5 pA/pF. The current magnitude declined after the peak to a steady-state level during the puff and decayed upon puff termination. Nominal removal of extracellular Ca^{2+} enhanced ~10-fold the IBMX-induced currents (peak amplitude: -41 ± 3.3 pA/pF, n=3) (Fig. 6B). Fig. 6C shows that IBMX reversibly depolarized the resting potential. Fig. 6D demonstrates that the currents were inward at negative holding potentials and outward at positive holding potentials. The estimated reversal potential of ~0 mV is consistent with a current supported by a cationic mixture.

CNGA3-dependent and -independent responses

We examined whether GG odorant responses persisted in *Cnga3*$^{-/-}$ mice. Histochemical experiments demonstrated a lack of ciliary immunoreactivity with a CNGA3-specific antibody in *Cnga3*$^{-/-}$ mice (Supplementary Fig. 5). GG neurons isolated from *Cnga3*$^{+/-}$ and *Cnga3*$^{-/-}$ littermates have similar intrinsic electrophysiological properties. GG neurons of *Cnga3*$^{-/-}$ mice exhibited all 3 spontaneous firing patterns (data not shown). In whole-cell recordings, GG neurons from *Cnga3*$^{-/-}$ mice exhibited the previously-reported (Chapter 3) extra-low voltage inactivating Na^+ current. Moreover, there were no significant differences in Na^+ current activation thresholds, I_h currents, or resting potentials between *Cnga3*$^{+/-}$ and *Cnga3*$^{-/-}$ mice (Supplementary Fig. 6). In extracellular recordings, neuronal exaltations were entirely absent with 20 s puffs of 1.3 mM 8-br-cGMP (n=17) (Fig. 7A,B) or 100 μM IBMX (n=12) (Fig. 7C,D) in *Cnga3*$^{-/-}$ mice. Thus, the depolarizing effects of increases in cyclic nucleotide concentration are fully mediated by CNGA3 channels.

Fig. 7E and 7F show examples of individual neurons from p0 *Cnga3*$^{+/-}$ and *Cnga3*$^{-/-}$ mice, respectively, in which 20 s puffs of 9.3 mM 2,5-DMP induced high-frequency bursts. This suggests that CNGA3 is not required for responses to 2,5-DMP in GG neurons. Overall, only 5/22 (23%) neurons responded in *Cnga3*$^{+/-}$ mice, and 2/17 (12%) responded in *Cnga3*$^{-/-}$ mice, within sampling error. As the *Cnga3*-mutant mouse line was in a RHJ/LeJ background (instead of BL/6/129), these results indicate some genetic background specificity in GG responses to 2,5-DMP. Inhibitory responses to 7.2 mM 2-heptanone were observed in the GG neurons of *Cnga3*$^{-/-}$ mice (Supplementary Fig. 2).

Responses to serum

We searched for other examples of biologically relevant GG stimuli. In routine histological examination of the nasal vestibule, we noticed that GG neurons were in proximity to a network of blood vessels (Fig. 8A). Fig. 8B shows that clusters of GG neurons could be within 5 μm of blood vessel walls that were positively stained for von Willebrand factor. The endothelial lining of the vasculature expressed PV-1 (Fig. 8C), a marker of the fenestrae that mediate vessel permeability in endocrine organs but not in the brain (Hallmann et al. 1995; Shue et al. 2008; Stan et al. 1999). Fig. 8D shows that a subset of the vessels was positively stained for the lymphatic marker LYVE1 (Banerji et al. 1999), suggesting that the vascular network in the nasal vestibule contains both lymphatic and blood vessels. The subsurface epithelium of the nasal vestibule is enriched with smooth muscle cells (Fig. 8E) that are likely innervated by sympathetic nerve varicosities that were positively stained for synaptophysin (Fig. 8F) and dopamine β-hydroxylase (Supplementary Fig. 7). Consistent with this idea, in electrophysiological slice recordings, we observed phasic and tonic vasoconstrictive movements in the vestibule when perfusing high K^+ and norepinephrine solutions, respectively (data not shown).

Compared to other olfactory subsystems, the GG has specialized vascular access. Fig. 9 shows the distribution of Evans blue (EB) dye in the nasal vestibule, MOE, and VNO across different methods of administration. Intraperitoneal injection of EB, which binds to serum albumin (Saria and Lundberg 1983), is a standard test of vascular permeability. In the microscopic examination of i.p.-injected animals

(Fig. 9A), the GG was strongly labeled with EB, whereas longer light exposures were needed to reveal EB in the epithelial sheets of the MOE and VNO (n=5). No dye was observed in the brain. In contrast, nasal irrigation of EB resulted in strong labeling of the MOE and the surface VNO, but lesser labeling of the nasal vestibule (n=4) (Fig. 9B). Untreated animals did not exhibit any appreciable signal (Fig. 9C).

Fig. 10A shows a mouse GG neuron that responded to a 20 s puff of diluted mouse serum with a decrease in firing rate. Overall, 17/24 (71%) neurons were inhibited by puffs of serum (Δf: -25 ± 6%, p3-p13). The effects had an exponential onset time constant of 3.3 ± 1.0 s and a decay time constant of 3.9 ± 1.0 s. All 3 spontaneous firing patterns were susceptible to alterations by serum. 20 s puffs of a high K^+ saline (osmotically balanced 30 mM KCl) showed that the serum effects were not due to ion imbalance, whose impacts have a faster time of onset (Supplementary Fig. 8). To determine what individual components of serum might be active, we considered that *in vivo* GG neurons are active in cold- (Mamasuew et al. 2008) and alarm-sensing (Brechbuhl et al. 2008) modalities, both situations of stress. Stress activates the hypothalamic-pituitary-adrenal axis to induce the adrenal-mediated secretion of cortisol or corticosterone into the blood. Fig. 10B demonstrates the inhibitory response of a GG neuron to a 20 s puff of 10 μM cortisol. A total of 7/15 (47%) neurons responded to 10 μM cortisol (Δf: -18 ± 2.3%, p5). In contrast, 20 s puffs of 150 μM norepinephrine did not affect spontaneous firing (n=5) (Fig. 10C-E).

DISCUSSION

Responses to odors and pheromones

In GG neurons, we demonstrated excitatory responses to 2,5-DMP and inhibitory responses to 2-heptanone and other general odorants. In general, these results support and extend *in vivo* experiments (Mamasuew et al. 2011a) that demonstrated c-Fos expression in GG neurons exposed to 2,5-DMP but not 2-heptanone. As c-Fos expression in neurons is not usually associated with reductions in firing rate, this assay would not be expected to detect odorant inhibition. Separately, we found that the pharmacological opening of a cGMP-gated cationic channel subunit CNGA3 mediates an excitatory effect. The increases

in firing rate likely underlie the Ca^{2+} bursts observed by Schmid and colleagues (Schmid et al. 2010). The electrophysiological properties of the IBMX-induced inward current, which is supported by CNGA3, include its inhibition by extracellular Ca^{2+} and a reversal potential near ~0 mV. These properties are consistent with previous descriptions of CNG channels in other systems (Frings et al. 1995).

The observed effects of 2,5-DMP on spontaneous firing across the 3 intrinsic discharge patterns are consistent with depolarization of the resting potential (Chapter 3). Future characterization of the size, time-dependence, and reversal potential of the membrane current will be necessary to understand its origin. Using the reported intra-pipette solutions, we were unable to obtain 2,5-DMP-induced currents in whole-cell recordings from GG neurons of p0 mice. A likely explanation is the fast dialysis of essential cellular components. Perforated patch recordings, used to study odor transduction in OSNs (Grosmaitre et al. 2006), will be beneficial.

As openings of CNGA3 channels increase firing rate in GG neurons, the channels are candidate proteins in an excitatory mechanism to explain the observed responses to 2,5-DMP. This is supported by *in vivo* studies with *Cnga3*$^{-/-}$ mice (Mamasuew et al. 2011b). However, in contrast to the *in vivo* data, we found that a minority of GG neurons in *Cnga3*$^{-/-}$ mice still exhibited transient elevations in firing rate when puffed with 2,5-DMP. Previous work has shown that OSNs can also detect 2,5-DMP in the absence of their cAMP-gated cationic channel subunit CNGA2 (Lin et al. 2004). An excitatory mechanism independent of cyclic nucleotide activity may exist in many different kinds of primary olfactory neurons and could commonly mediate detection of 2,5-DMP. In support of this, OSNs exhibit reduced responsiveness to 2,5-DMP in the presence of pharmacological inhibitors of phospholipase C (Lin et al. 2004).

The dose-response relationship of GG neurons to 2,5-DMP and 2,3-DMP is in the millimolar range. Collagenase treatment of nasal vestibule slices may have affected some surface odor recognition proteins. The millimolar dose-response curve contrasts with the observed curve in VSNs, which can detect 2,5-DMP at nanomolar concentrations (Leinders-Zufall et al. 2000), and is at least 3 orders of magnitude higher than the estimated concentration of individual pheromones in female urine (Novotny et

al. 2007). Moreover, the responses in the GG are strongest in neonatal mice, which are not sexually mature. Thus, even though 2,5-DMP can impact the reproductive cycles of rodents, the role played by the GG in this process is presently unclear. One possibility is that the activity of only several GG neurons is sufficient to trigger downstream effects in the adult. On a cellular level, a small subset of GG neurons may exhibit exceptional sensitivity to 2,5-DMP; individual VSNs have heterogeneous dose-response relationships to 2,5-DMP that vary over 4 orders of magnitude (He et al. 2010). A second possibility is that the detection of 2,5-DMP has physiological importance throughout (and possibly before) life, but that the function of the GG is only needed at neonatal ages. A third possibility is that GG neurons in neonates retain the broad chemoresponsive profile of a "common" OSN or OSN precursor, but that developmental changes toward specialization in the first several days of life remove an artifactual sensitivity to 2,5-DMP.

In order for an odorant to excite a GG neuron, its excitatory driving force must be greater than its relatively non-selective inhibitory driving force. The inhibitory effects of 2-heptanone and a few other odorants are intriguing due to the presence of a distinct Na^+ channel that is activated at hyperpolarized potentials in GG neurons (Chapter 3). Spontaneous APs at moderate concentrations of these odorants would be expected to mobilize a greater fraction of this unusual Na^+ current. In OSNs, conductance through a second Na^+ channel is required for odor transduction along axons to the olfactory bulb (Weiss et al. 2011). Alternatively, as many GG neurons exhibit high (>10 Hz) rates of spontaneous firing, inhibitory signals may have greater salience than desensitizing excitatory ones.

It is possible that 2-heptanone and other tested odorants are recognized by a broadly tuned odorant receptor (Duchamp-Viret et al. 1999). This receptor may be coupled to signal transduction elements whose final output is to induce membrane hyperpolarization. The inhibitory effects of single odorants observed in this study may be an extension of a general odorant-inhibition phenomenon. Odorant-induced hyperpolarization is also a feature of mammalian OSNs and is dependent on CNGA2 (Delay and Restrepo 2004). In our experiments on the GG, the inhibition by 2-heptanone was retained

even with removal of CNGA3. Most GG neurons do not express CNGA2 (Roppolo et al. 2006). Thus, odorant-induced hyperpolarization in the GG is likely mediated by a distinct mechanism.

The currents induced by 2-heptanone have a reversal potential of approximately -85 mV. As demonstrated in Fig. 4D, at positive holding potentials the currents could be as large as 400 pA, suggesting the movement of ions with a large electrochemical gradient. Thus, in GG neurons 2-heptanone likely increases the conductance of a K^+ channel. Because K^+ channels have multiple routes for modulation (Dilly et al. 2011), one explanation for these results is that the tested odorants either directly or indirectly (through a nonspecific chemical or physical property) interact with the K^+ channel. The odorant-induced inhibition was not a result of osmolarity or pH changes. It is also unlikely to be due to vapor pressure, as ethanol, which has a higher vapor pressure than 2-heptanone, induced only a modest inhibitory response at ~9 mM. Because odorants are often hydrophobic, lipophilicity may represent a key factor in the observed sensitivity of the inhibitory response.

Responses to serum

With the exception of 2-heptanol, whose inhibitory effects could be discerned at 150 μM, millimolar concentrations of odorants were required to observe responses in the GG. This raises the question of whether the inhibitory responses have any physiological relevance. We therefore searched for examples of biologically relevant compounds at near-physiological concentrations that could affect spontaneous activity in the GG. To this end, we found that GG neurons reside in a dense bed of blood and lymphatic vessels and are highly susceptible to vasoactive movements of autonomic origin. Injections of Evans blue dye revealed strong labeling of the nasal vestibule epithelium and weaker labeling of the MOE and VNO. These experiments suggest that neuronal activity in the GG is vulnerable to modulation by serum contents, in contrast to OSNs and vomeronasal sensory neurons.

Consistent with this hypothesis, serum reduced firing rate in the majority of GG neurons, even in neurons from a p13 mouse. We do not know if the sum of all the components in serum caused the inhibitory response and thus represents a more-native measure of spontaneous activity in the GG, or if the

serum contained one or several components of exceptional relevance, which were triggered by the presumptive animal stress during the serum isolation procedure. Nonetheless, the results suggest that inhibitory responses in the GG can be elicited by chemicals at biologically relevant concentrations.

This is not to suggest that GG neurons exclusively sample internally circulating molecules. Pheromones and hormones are found in both serum and urine (Nodari et al. 2008; Novotny et al. 2007). The far-anterior location of the ganglion should indicate that the neurons are well positioned to be the first olfactory subsystem to interrogate inhaled odorants. However, an intriguing possibility is that specific molecules in serum, by inhibiting GG neurons, may be able to nullify the responses induced by the simultaneous inhalation of excitatory odorants. The GG may therefore have the capability to calibrate autonomously its sensory sensitivity with the internal physiological status of the animal.

A potential physiological state that can modulate GG activity is stress, as previous studies have indicated a role for the GG in mediating alarm behavior (Brechbuhl et al. 2008). Stress-responsiveness in GG neurons would be conferred by a different mechanism. We found that 10 μM cortisol inhibited spontaneous firing nearly half of the tested neurons, whereas 150 μM norepinephrine had no effect. Cortisol has short-term effects on neuronal firing in other systems (Avanzino et al. 1987; Avanzino et al. 1984; Filaretov 1976; Kasai et al. 1988; Zaki and Barrett-Jolley 2002). Membrane-permeable glucocorticoids are well suited to be endogenous modulators of GG activity. Because GG neurons are ensheathed by glial cells, modulators of GG activity are likely to be gaseous or lipid-soluble. During periods of extreme stress in rodents, levels of free glucocorticoids in serum can be as high as 3 μM (Bassett et al. 1978). Other factors in serum, such as binding proteins, may increase the sensitivity of GG neurons to glucocorticoids. Previous *in vivo* work on the GG may have inadvertently revealed on the detection of stress-related compounds in the bloodstream, as naris occlusions did not eliminate the neuronal activity (Brechbuhl et al. 2008; Mamasuew et al. 2008). Triggers such as alarm pheromones and cold may be primarily detected by other sensory systems and invoke GG activity as a secondary consequence. Future studies should be directed at evaluating whether serum modulation of GG activity has any significance *in vivo*.

ACKNOWLEDGMENTS

We thank B. Chang for *Cnga3*$^{-/-}$ mice. We thank J. Gutierrez for animal husbandry. This project was supported by grants from the U.S. National Institutes of Health and the U.S. National Science Foundation.

CONTRIBUTIONS

C.Y.L. and D.S.K. performed experiments. D.S.K., C.X., H.A.L., and S.E.F. contributed equipment and guided experiments. C.Y.L. wrote the paper.

REFERENCES

Avanzino GL, Ermirio R, Cogo CE, Ruggeri P, and Molinari C. Effects of corticosterone on neurones of the locus coeruleus, in the rat. *Neurosci Lett* 80: 85-88, 1987.

Avanzino GL, Ermirio R, Ruggeri P, and Cogo CE. Effect of microelectrophoretically applied corticosterone on raphe neurones in the rat. *Neurosci Lett* 50: 307-311, 1984.

Banerji S, Ni J, Wang SX, Clasper S, Su J, Tammi R, Jones M, and Jackson DG. LYVE-1, a new homologue of the CD44 glycoprotein, is a lymph-specific receptor for hyaluronan. *J Cell Biol* 144: 789-801, 1999.

Bassett JR, Strand FL, and Cairncross KD. Glucocorticoids, adrenocorticotropichormone and related polypeptides on myocardial sensitivity to noradrenaline. *Eur J Pharmacol* 49: 243-249, 1978.

Brechbuhl J, Klaey M, and Broillet MC. Grueneberg ganglion cells mediate alarm pheromone detection in mice. *Science* 321: 1092-1095, 2008.

Delay R, and Restrepo D. Odorant responses of dual polarity are mediated by cAMP in mouse olfactory sensory neurons. *J Neurophysiol* 92: 1312-1319, 2004.

Dilly S, Lamy C, Marrion NV, Liegeois JF, and Seutin V. Ion-channel modulators: more diversity than previously thought. *Chembiochem* 12: 1808-1812, 2011.

Duchamp-Viret P, Chaput MA, and Duchamp A. Odor response properties of rat olfactory receptor neurons. *Science* 284: 2171-2174, 1999.

Filaretov AA. The afferent input and functional organization of the hypothalamus in reactions regulating pituitary-adreno-cortical activity. *Brain Res* 107: 39-54, 1976.

Fleischer J, Hass N, Schwarzenbacher K, Besser S, and Breer H. A novel population of neuronal cells expressing the olfactory marker protein (OMP) in the anterior/dorsal region of the nasal cavity. *Histochem Cell Biol* 125: 337-349, 2006.

Fleischer J, Mamasuew K, and Breer H. Expression of cGMP signaling elements in the Grueneberg ganglion. *Histochem Cell Biol* 131: 75-88, 2009.

Frings S, Seifert R, Godde M, and Kaupp UB. Profoundly different calcium permeation and blockage determine the specific function of distinct cyclic nucleotide-gated channels. *Neuron* 15: 169-179, 1995.

Fuss SH, Omura M, and Mombaerts P. The Grueneberg ganglion of the mouse projects axons to glomeruli in the olfactory bulb. *Eur J Neurosci* 22: 2649-2654, 2005.

Grosmaitre X, Vassalli A, Mombaerts P, Shepherd GM, and Ma M. Odorant responses of olfactory sensory neurons expressing the odorant receptor MOR23: a patch clamp analysis in gene-targeted mice. *Proc Natl Acad Sci U S A* 103: 1970-1975, 2006.

Grüneberg H. A ganglion probably belonging to the N. terminalis system in the nasal mucosa of the mouse. *Z Anat Entwicklungsgesch* 140: 39-52, 1973.

Hallmann R, Mayer DN, Berg EL, Broermann R, and Butcher EC. Novel mouse endothelial cell surface marker is suppressed during differentiation of the blood brain barrier. *Dev Dyn* 202: 325-332, 1995.

He J, Ma L, Kim S, Schwartz J, Santilli M, Wood C, Durnin MH, and Yu CR. Distinct signals conveyed by pheromone concentrations to the mouse vomeronasal organ. *J Neurosci* 30: 7473-7483, 2010.

Kasai M, Kannan H, Ueta Y, Osaka T, Inenaga K, and Yamashita H. Effects of iontophoretically applied cortisol on tuberoinfundibular neurons in hypothalamic paraventricular nucleus of anesthetized rats. *Neurosci Lett* 87: 35-40, 1988.

Koos DS, and Fraser SE. The Grueneberg ganglion projects to the olfactory bulb. *Neuroreport* 16: 1929-1932, 2005.

Leinders-Zufall T, Lane AP, Puche AC, Ma W, Novotny MV, Shipley MT, and Zufall F. Ultrasensitive pheromone detection by mammalian vomeronasal neurons. *Nature* 405: 792-796, 2000.

Lin W, Arellano J, Slotnick B, and Restrepo D. Odors detected by mice deficient in cyclic nucleotide-gated channel subunit A2 stimulate the main olfactory system. *J Neurosci* 24: 3703-3710, 2004.

Liu CY, Fraser SE, and Koos DS. Grueneberg ganglion olfactory subsystem employs a cGMP signaling pathway. *J Comp Neurol* 516: 36-48, 2009.

Mamasuew K, Breer H, and Fleischer J. Grueneberg ganglion neurons respond to cool ambient temperatures. *Eur J Neurosci* 28: 1775-1785, 2008.

Mamasuew K, Hofmann N, Breer H, and Fleischer J. Grueneberg ganglion neurons are activated by a defined set of odorants. *Chem Senses* 36: 271-282, 2011a.

Mamasuew K, Hofmann N, Kretzschmann V, Biel M, Yang RB, Breer H, and Fleischer J. Chemo- and thermosensory responsiveness of Grueneberg ganglion neurons relies on cyclic guanosine monophosphate signaling elements. *Neurosignals* 19: 198-209, 2011b.

Mamasuew K, Michalakis S, Breer H, Biel M, and Fleischer J. The cyclic nucleotide-gated ion channel CNGA3 contributes to coolness-induced responses of Grueneberg ganglion neurons. *Cell Mol Life Sci* 67: 1859-1869, 2010.

Nodari F, Hsu FF, Fu X, Holekamp TF, Kao LF, Turk J, and Holy TE. Sulfated steroids as natural ligands of mouse pheromone-sensing neurons. *J Neurosci* 28: 6407-6418, 2008.

Novotny M, Jemiolo B, Harvey S, Wiesler D, and Marchlewska-Koj A. Adrenal-mediated endogenous metabolites inhibit puberty in female mice. *Science* 231: 722-725, 1986.

Novotny MV, Soini HA, Koyama S, Wiesler D, Bruce KE, and Penn DJ. Chemical identification of MHC-influenced volatile compounds in mouse urine. I: Quantitative Proportions of Major Chemosignals. *J Chem Ecol* 33: 417-434, 2007.

Potter SM, Zheng C, Koos DS, Feinstein P, Fraser SE, and Mombaerts P. Structure and emergence of specific olfactory glomeruli in the mouse. *J Neurosci* 21: 9713-9723, 2001.

Riviere S, Challet L, Fluegge D, Spehr M, and Rodriguez I. Formyl peptide receptor-like proteins are a novel family of vomeronasal chemosensors. *Nature* 459: 574-577, 2009.

Roppolo D, Ribaud V, Jungo VP, Luscher C, and Rodriguez I. Projection of the Gruneberg ganglion to the mouse olfactory bulb. *Eur J Neurosci* 23: 2887-2894, 2006.

Saria A, and Lundberg JM. Evans blue fluorescence: quantitative and morphological evaluation of vascular permeability in animal tissues. *J Neurosci Methods* 8: 41-49, 1983.

Schmid A, Pyrski M, Biel M, Leinders-Zufall T, and Zufall F. Grueneberg ganglion neurons are finely tuned cold sensors. *J Neurosci* 30: 7563-7568, 2010.

Shue EH, Carson-Walter EB, Liu Y, Winans BN, Ali ZS, Chen J, and Walter KA. Plasmalemmal vesicle associated protein-1 (PV-1) is a marker of blood-brain barrier disruption in rodent models. *BMC Neurosci* 9: 29, 2008.

Stan RV, Kubitza M, and Palade GE. PV-1 is a component of the fenestral and stomatal diaphragms in fenestrated endothelia. *Proc Natl Acad Sci U S A* 96: 13203-13207, 1999.

Storan MJ, and Key B. Septal organ of Gruneberg is part of the olfactory system. *J Comp Neurol* 494: 834-844, 2006.

Weiss J, Pyrski M, Jacobi E, Bufe B, Willnecker V, Schick B, Zizzari P, Gossage SJ, Greer CA, Leinders-Zufall T, Woods CG, Wood JN, and Zufall F. Loss-of-function mutations in sodium channel Nav1.7 cause anosmia. *Nature* 472: 186-190, 2011.

Zaki A, and Barrett-Jolley R. Rapid neuromodulation by cortisol in the rat paraventricular nucleus: an in vitro study. *Br J Pharmacol* 137: 87-97, 2002.

TABLES

Table 1: GG inhibitory responses elicited by puffs of 5-10 mM odorants in p2-p5 mice.

Chemical	mM (*n*)	Δ*f*, %
2-heptanol	7.1 (2)	-99 ± 1.1
citral	5.8 (4)	-98 ± 0.9
2-heptanone	7.2 (5)	-85 ± 14
eucalyptol	6.0 (5)	-77 ± 11
pyrazine	10 (10)	-59 ± 12
isovaleric acid	1.0 (5)*	-25 ± 19
ethanol	8.6 (7)	-18 ± 9.2
DMSO	7.0 (9)	+4.8 ± 3.8
D-glucose	10 (3)	+0.6 ± 4.9

* Higher concentrations of isovaleric acid induced acidity-related artifacts (Supplementary Fig. 3).

FIGURE LEGENDS

Figure 1: GG neurons in an acute slice preparation. The chemosensory capabilities of mouse Grueneberg ganglion (GG) neurons were investigated with pressure ejections ("puffs") of odorants. A) GG neurons could be identified by their green fluorescence in OMP-GFP$^{+/-}$ mice. The pipette on the left is the patch pipette. The pipette on the right is the puff pipette that delivered the chemicals of interest. B) Frequency vs. time plot of the spontaneous firing in a GG neuron. The horizontal black line on the top of the graph indicates the onset and duration of a puff of saline. The spontaneous firing of GG neurons is not altered by puffs of saline. Scale bar: 50 μm.

Figure 2: GG neurons from neonatal mice respond to 9.3 mM 2,5-DMP. A) The spontaneous discharge of a phasic-firing GG neuron (top panel) is composed of bursts of action potential (AP) spikes. During a puff of 2,5-DMP (region 1), the firing frequency within a burst increases (lower left panel), compared to the frequency before (region 1) and after (region 3) the puff. In this same neuron, a frequency vs. time plot (lower right panel) clearly marks the reversible increase in the intraburst frequency induced by 2,5-DMP. B) 2,5-DMP in a RSS-firing neuron increases the total firing rate. The instantaneous firing rate is fit to a two-exponential functional form (inset) to account for desensitization during a 20 s puff. C) In a sporadic-firing neuron, 2,5-DMP caused a transient set of high-frequency spikes. Horizontal black lines indicate puff onset and duration.

Figure 3: Population parameters of responsive neonatal GG neurons to 2,5-DMP. A) Depicted is the median time course (black line) of the response during a 20 s puff. A desensitization of >90% is observed during the puff. Individual responses are shown in the gray dotted lines. B) GG neurons from p0 mice were puffed with various concentrations (1.9, 4.6, 9.3 mM) of 2,5-DMP, revealing the dose dependence of their responses. C) p0-p4 mice were puffed with 9.3 mM 2,5-DMP. The responses declined with increasing age. The dotted line shows an exponential decay fit to the data.

D) GG neurons responded to 2,3-DMP with dose-dependent excitations.

Figure 4: GG neurons exhibit inhibitory responses to 3.6 mM 2-heptanone. A-C) on-cell recordings. D-E) whole-cell recordings. A) 5 s puffs (horizontal black line) of 2-heptanone induce abrupt and reversible decreases in the frequency of spontaneous charge in an RSS-firing neuron. B) The frequency vs. time plot of the neuron shown in (A) supports the aforementioned inhibition. C) The effects of 2-heptanone were dose dependent and had an IC_{50} of ~2 mM. D) Depicted are 5 s puffs of 7.2 mM 2-heptanone on a neuron clamped at different holding potentials. Associated with the puff is an outward current that increases in magnitude at more positive holding potentials. E) A 20 s puff of 2-heptanone induced a reversible hyperpolarization of the resting potential in a GG neuron.

Figure 5: Small-molecule modulators of the cGMP pathway induce excitatory responses in GG neurons. A) 20 s puffs (horizontal black lines) of 1.3 mM membrane-permeant 8-br-cGMP cause neuronal exaltations. B) A frequency vs. time plot of an RSS-firing neuron shows the rise and decay of the 8-br-cGMP-induced effect. The insets show exponential fits to the rise and decay, used to derive the time constants described in the text. C) Puffs of 100 μM IBMX elicited excitatory responses in some GG neurons. D) In other neurons, IBMX caused a transient burst of high-frequency spikes followed by a decrease in the overall firing rate. The burst is shown in the left panel; the right panel depicts the frequency vs. time plot for this neuron.

Figure 6: The cyclic nucleotide pathway can elicit membrane currents and alter resting potential. A) A 20 s puff of IBMX from a holding potential of -64 mV elicits inward currents. The currents exhibited both transient and sustained components. B) Nominal removal of Ca^{2+} enlarges IBMX-induced currents ~10-fold. C) Inward currents correlate with a depolarization of the resting potential. D) IBMX was puffed onto a GG neuron that successively clamped at more-positive holding potentials. The inset shows the I-V relationship of the elicited currents and indicates a reversal potential of ~0 mV.

Figure 7: CNGA3 is essential for neuronal responses induced by cyclic nucleotides. Shown are representative frequency vs. time plots of puffs of 1.3 mM 8-br-cGMP (A,B), 100 μM IBMX (C,D), and 9.3 mM 2,5-DMP (E,F) in *Cnga3*$^{+/-}$ (A,C,E) and *Cnga3*$^{-/-}$ (B,D,F) littermates. Horizontal blank lines indicate puff onset and duration. Responses to 8-br-cGMP and IBMX were completely absent in *Cnga3*$^{-/-}$ mice.

Figure 8: GG neurons reside near a vascular bed. A) Brightfield image (red) overlaid with green fluorescent signal shows that GG neurons reside at the anterior terminus of a nasal vascular plexus. B-D) Stainings on thin sections of the nasal vestibule for B) von Willebrand factor (vWF), C) plasmalemmal vesicular associated protein (PV-1), D) lymphatic LYVE1 and CD31/PECAM-1, and E) smooth muscle actin (αSMA). F) Whole-mount staining for synaptophysin (Syp) demonstrates axon varicosities of likely-sympathetic origin in the nasal vestibule. Scale bars: A) 400 μm, B) 50 μm, C) 60 μm, D) 100 μm, E) 50 μm, F) 40 μm.

Figure 9: GG neurons have preferential vascular access. A) Intraperitoneal (i.p.) injections of Evans blue (EB) dye resulted in preferential labeling of the nasal vestibule but not the epithelial layer of the MOE and VNO olfactory organs. Inset shows sagittal view of bisected nasal cavity under white light with rightmost portion representing the olfactory bulb and leftmost portion representing the respiratory epithelium. EB signal in fluorescent microscopic images is false-colored white. GFP signal of OMP-GFP mice is in green. A large amount of EB could inhibit the local GFP signal. B) Nasal irrigation of EB preferentially labels the MOE and VNO. C) There was minimal autofluorescence in the nasal vestibule, MOE, and VNO of un-manipulated mice. Scale bars: 200 μm, 2 mm (inset).

Figure 10: Potential compounds in serum alter GG activity. 20 s puffs of A) mouse serum and B) 10 μM cortisol reduce overall firing rate in GG neurons. C-E) Frequency vs. time plots of firing in GG neurons

puffed with C) serum, D) 10 μM cortisol, and E) 150 μM norepinephrine. Horizontal black bars indicate puff onset and duration.

FIGURES

Figure 1:

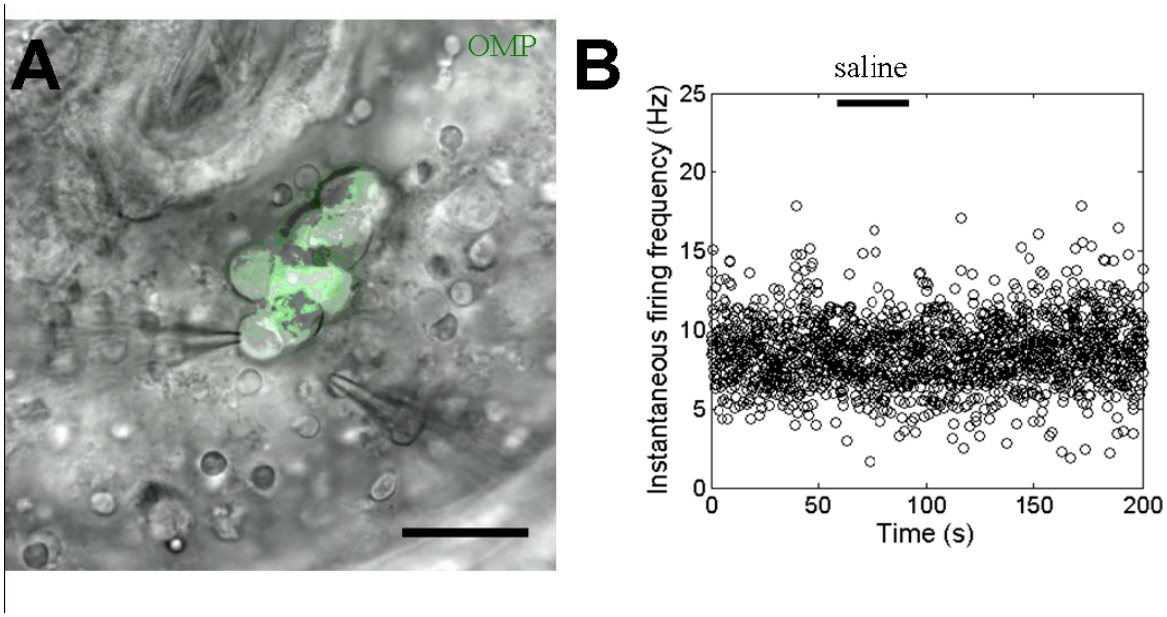

Figure 2:

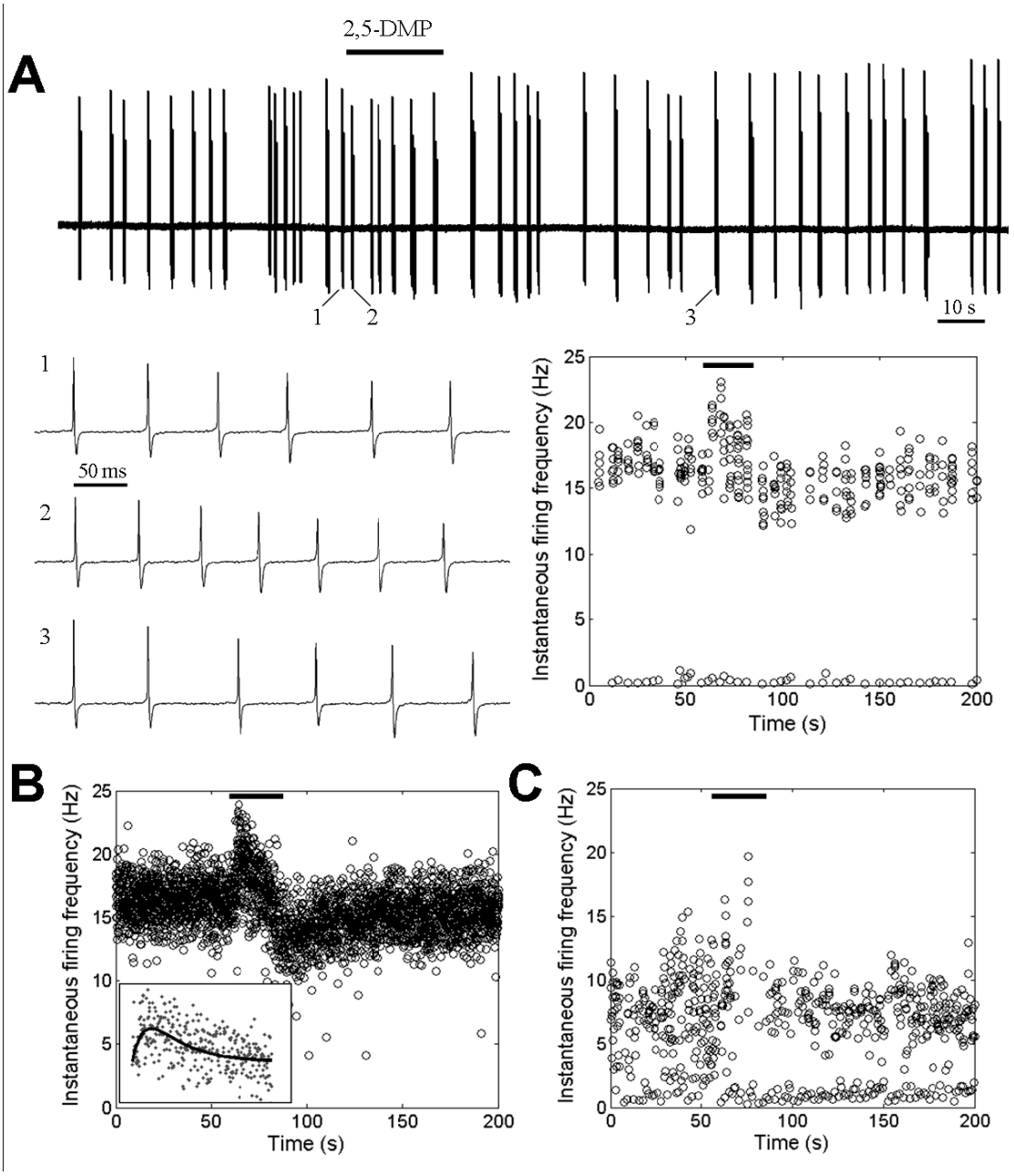
A
2,5-DMP
1
2
3
10 s
1
50 ms
2
3
Instantaneous firing frequency (Hz)
Time (s)
B
C
Instantaneous firing frequency (Hz)
Time (s)
Instantaneous firing frequency (Hz)
Time (s)

Figure 3:

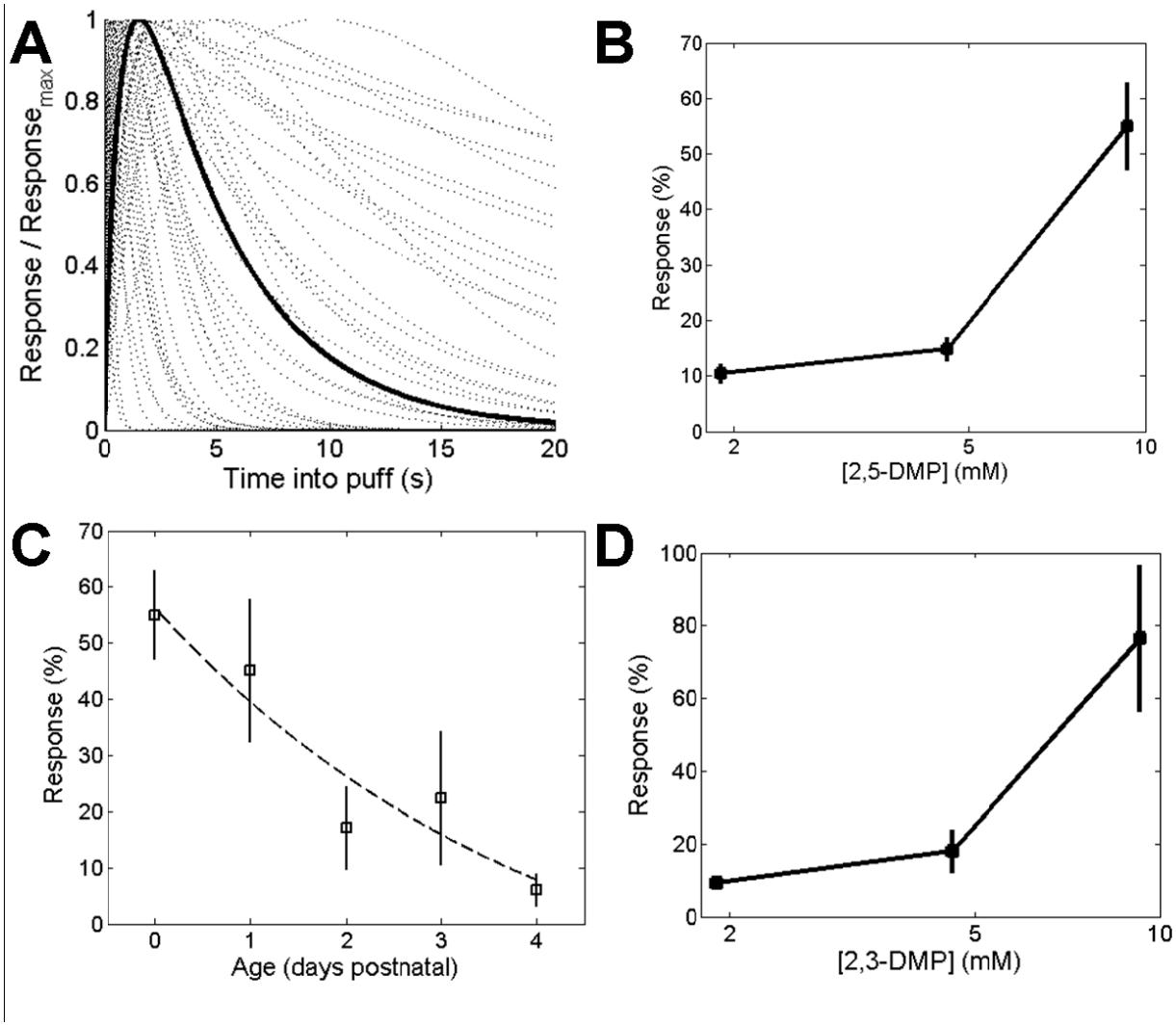
A
Response / Response$_{max}$
Time into puff (s)
B
Response (%)
[2,5-DMP] (mM)
C
Response (%)
Age (days postnatal)
D
Response (%)
[2,3-DMP] (mM)

Figure 4:

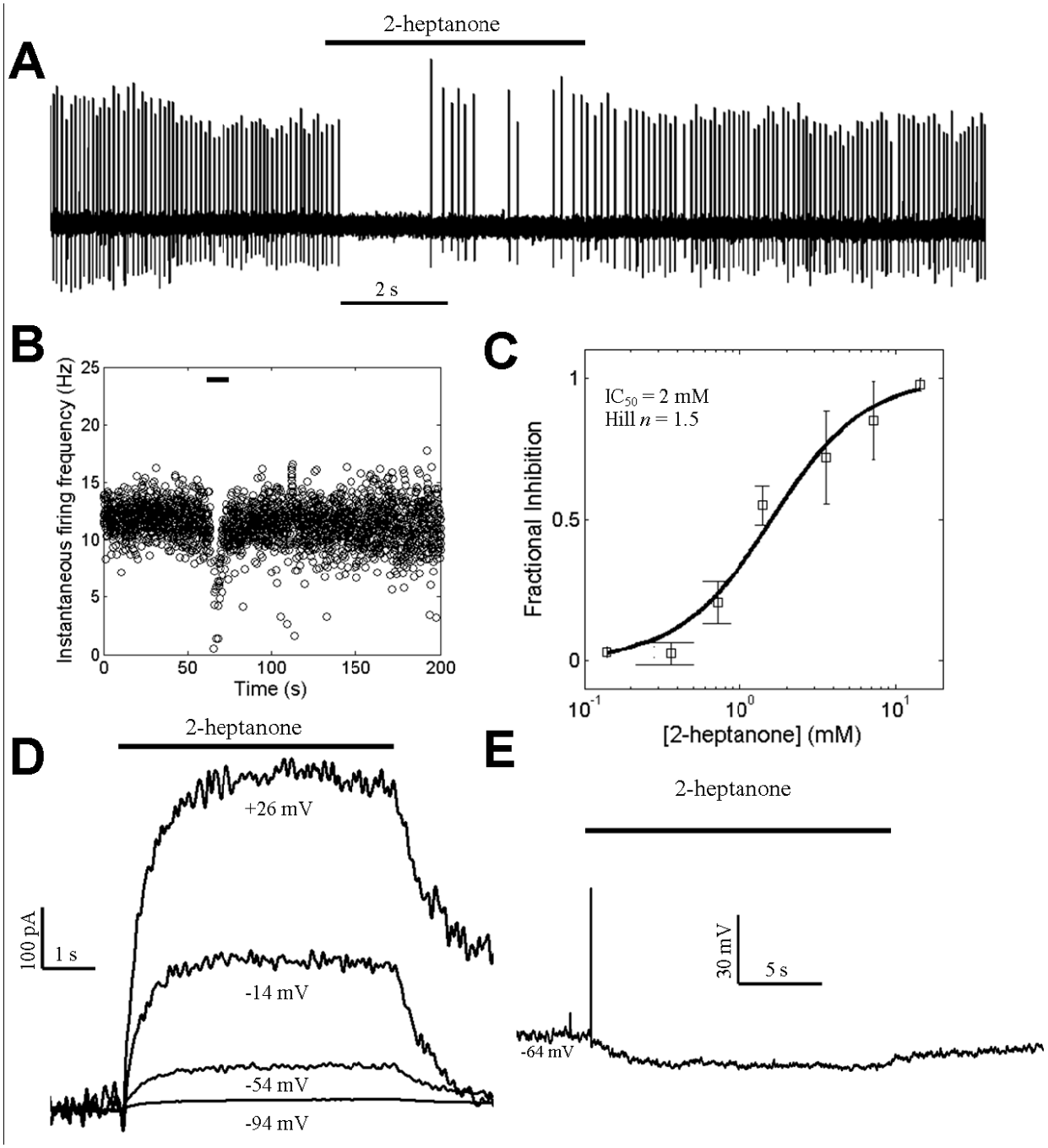
A
2-heptanone
2 s
B
Instantaneous firing frequency (Hz)
Time (s)
C
Fractional Inhibition
IC50 = 2 mM
Hill n = 1.5
[2-heptanone] (mM)
D
2-heptanone
+26 mV
-14 mV
-54 mV
-94 mV
100 pA
1 s
E
2-heptanone
30 mV
5 s
-64 mV

Figure 5:

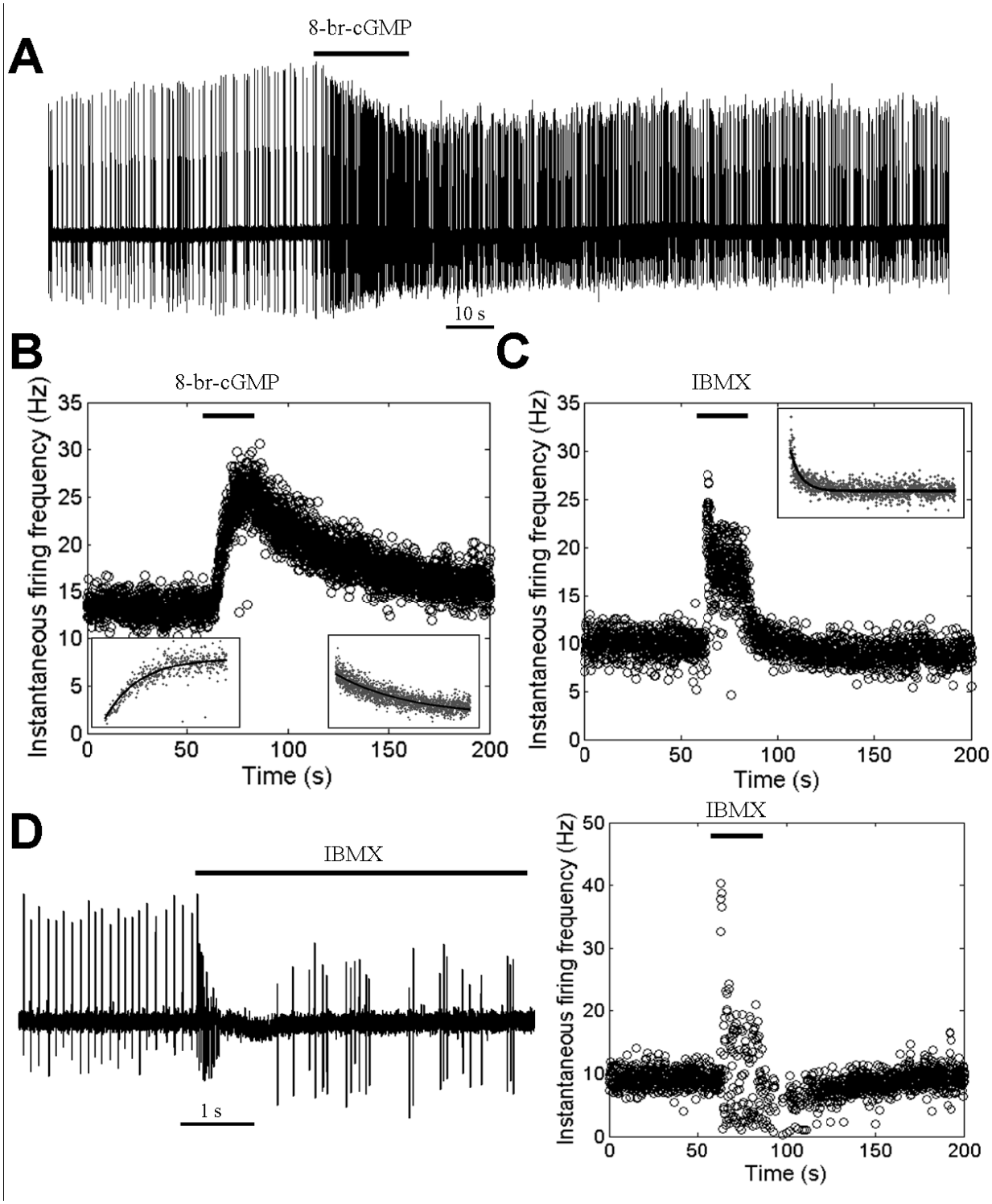
A
8-br-cGMP
10 s
B
8-br-cGMP
Instantaneous firing frequency (Hz)
Time (s)
C
IBMX
Instantaneous firing frequency (Hz)
Time (s)
D
IBMX
1 s
IBMX
Instantaneous firing frequency (Hz)
Time (s)

Figure 6:

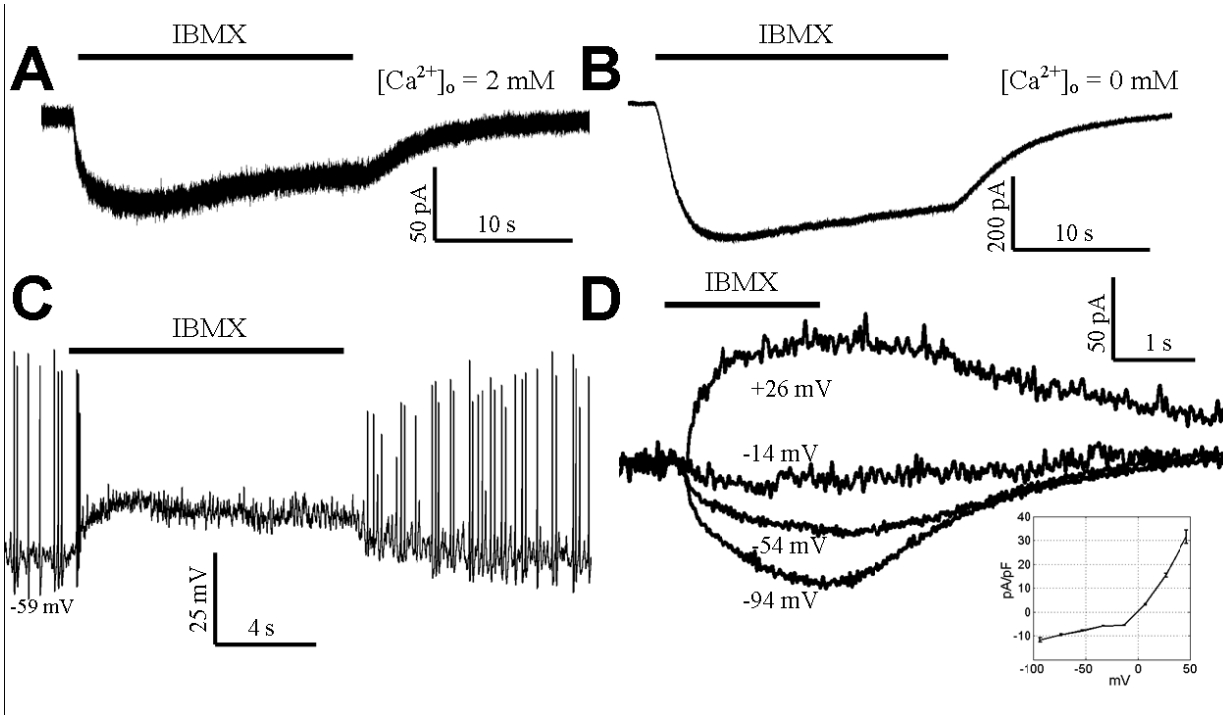
A
IBMX
[Ca2+]o = 2 mM
50 pA
10 s
B
IBMX
[Ca2+]o = 0 mM
200 pA
10 s
C
IBMX
-59 mV
25 mV
4 s
D
IBMX
50 pA
1 s
+26 mV
-14 mV
-54 mV
-94 mV
pA/pF
mV

Figure 7:

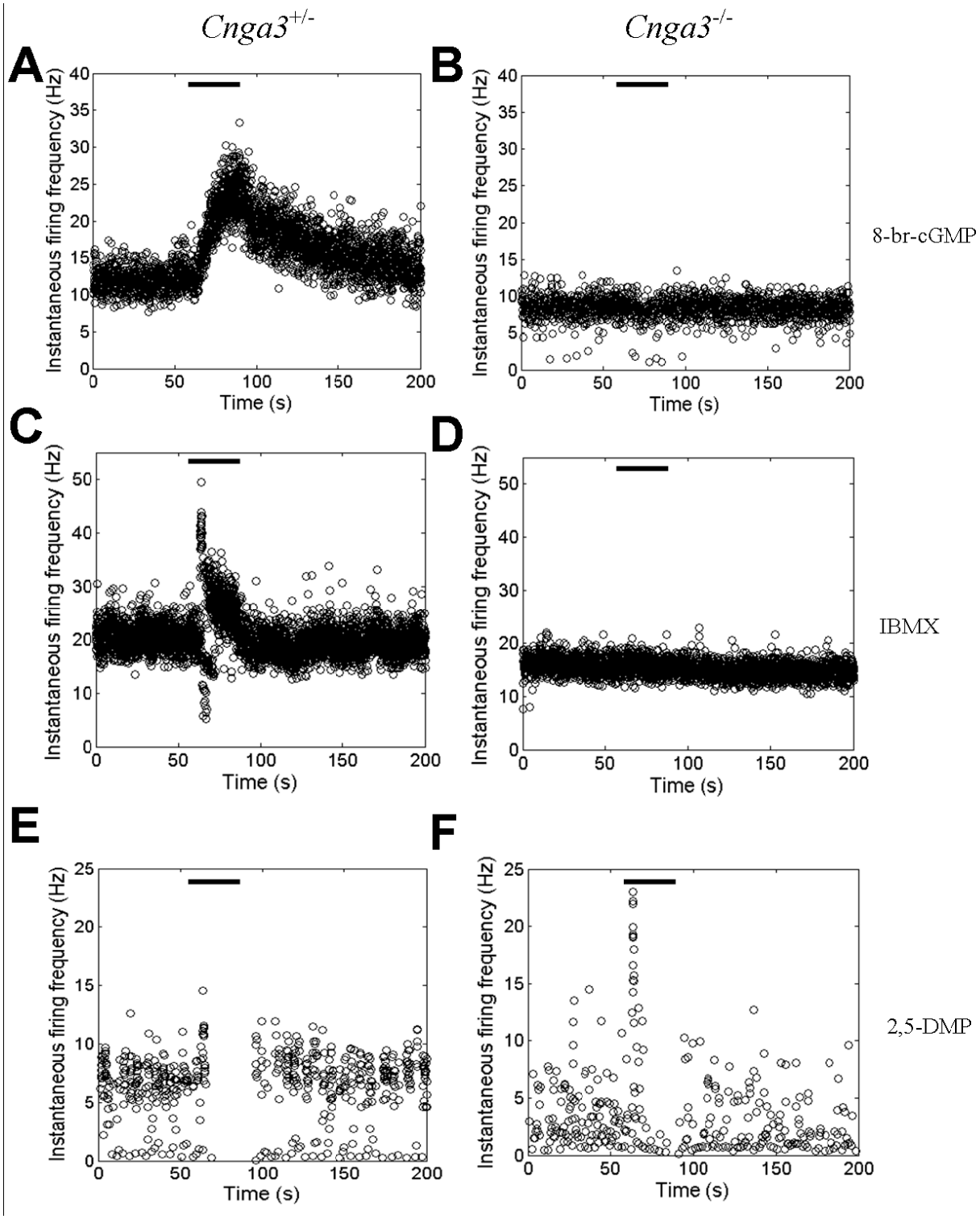
Cnga3+/-
Cnga3-/-
A
B
C
D
E
F
Instantaneous firing frequency (Hz)
Time (s)
8-br-cGMP
IBMX
2,5-DMP

Figure 8:

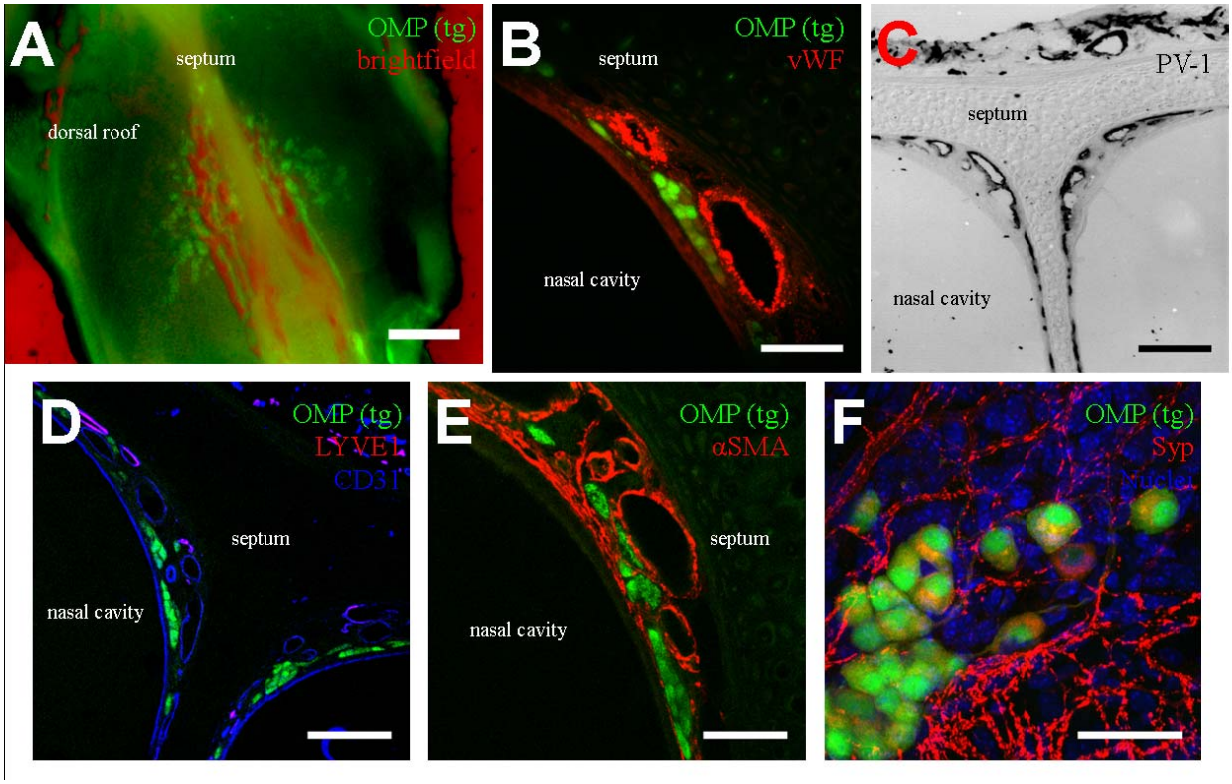
A
OMP (tg)
brightfield
septum
dorsal roof
B
OMP (tg)
vWF
septum
nasal cavity
C
PV-1
septum
nasal cavity
D
OMP (tg)
LYVE1
CD31
septum
nasal cavity
E
OMP (tg)
αSMA
septum
nasal cavity
F
OMP (tg)
Syp
Nuclei

Figure 9:

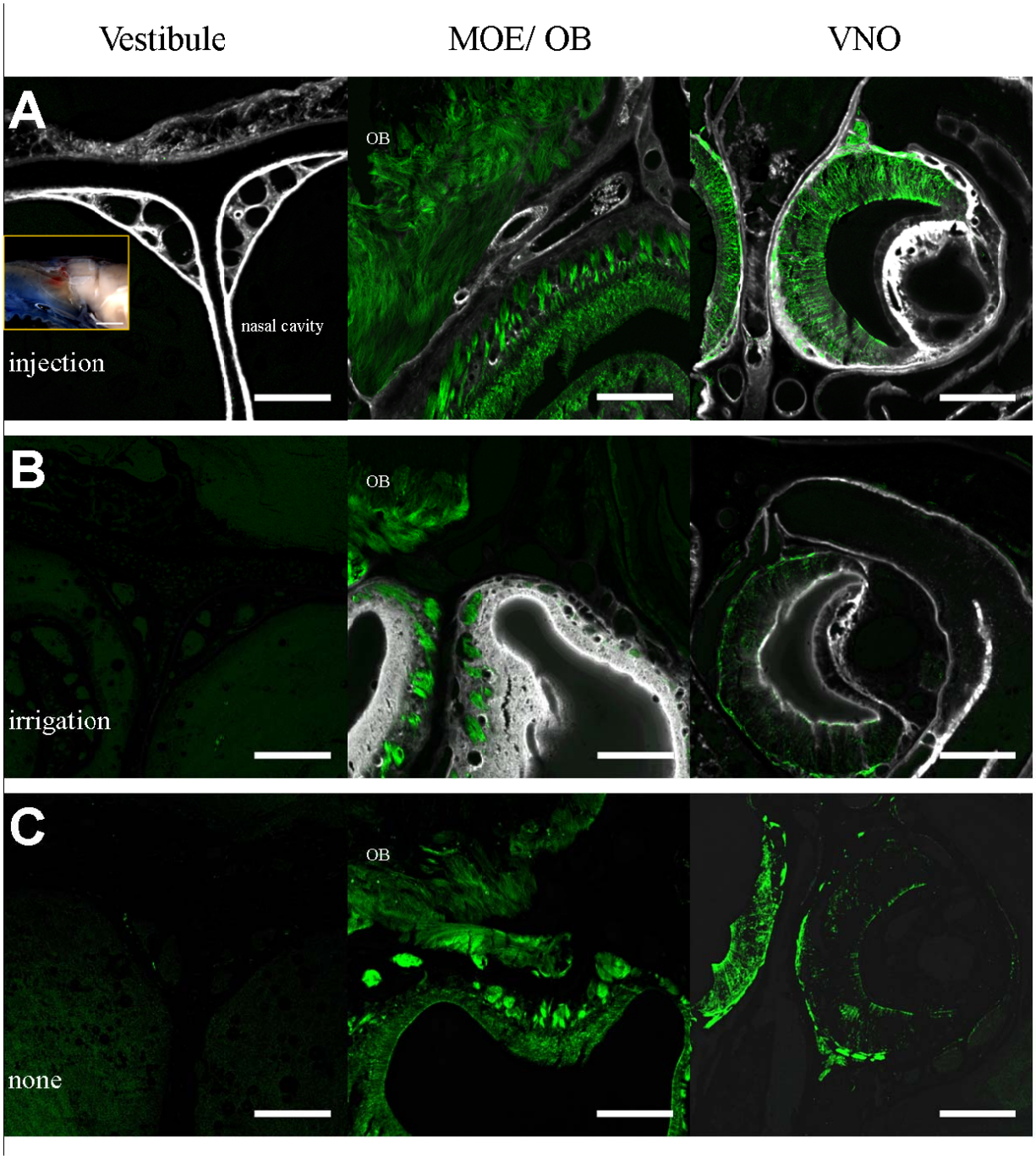
Vestibule
MOE/ OB
VNO
A
OB
nasal cavity
injection
B
OB
irrigation
C
OB
none

Figure 10:

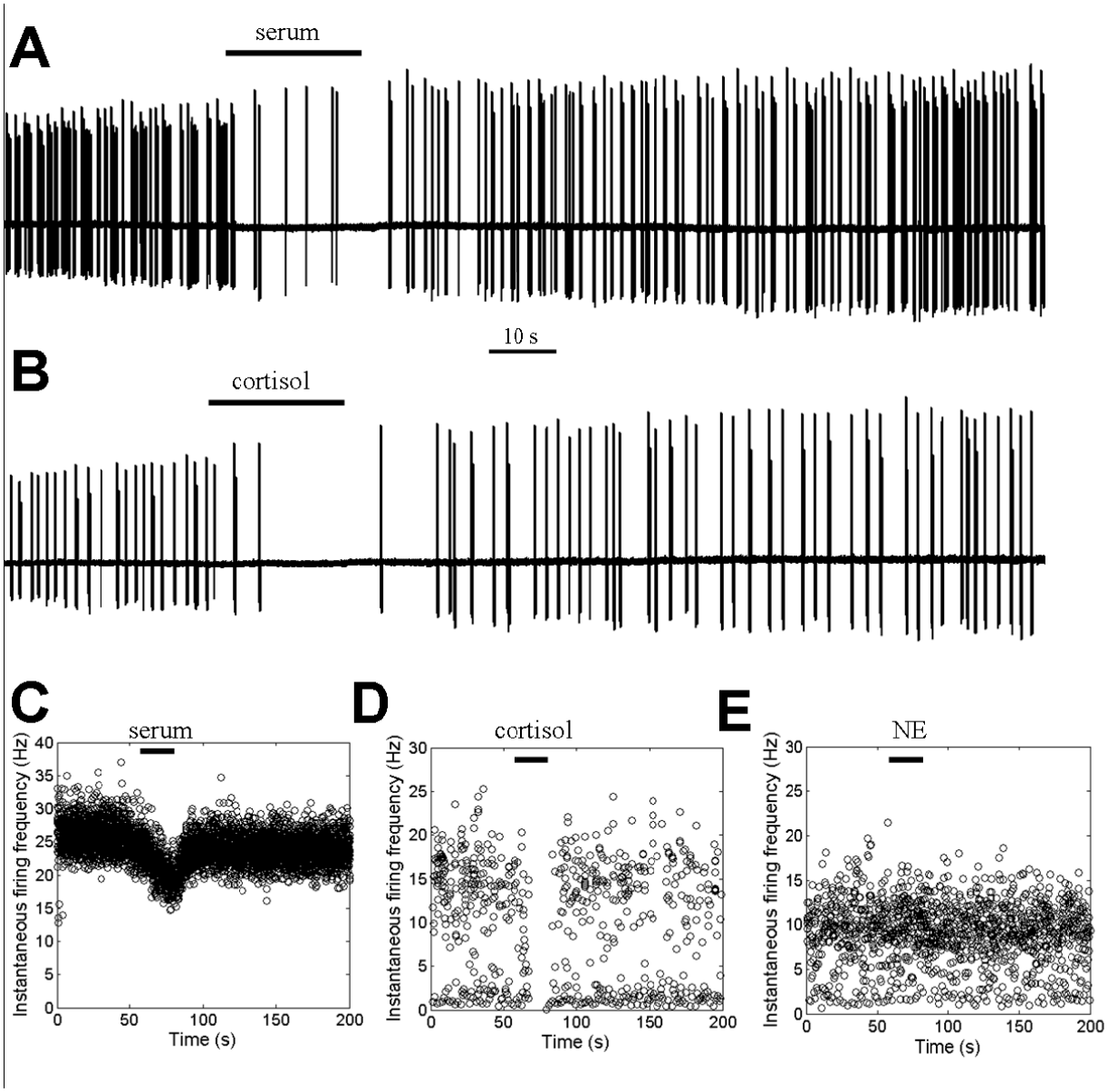
A
serum
10 s
B
cortisol
C
serum
D
cortisol
E
NE
Instantaneous firing frequency (Hz)
Time (s)

SUPPLEMENTARY FIGURES

Supplementary Figure 1:

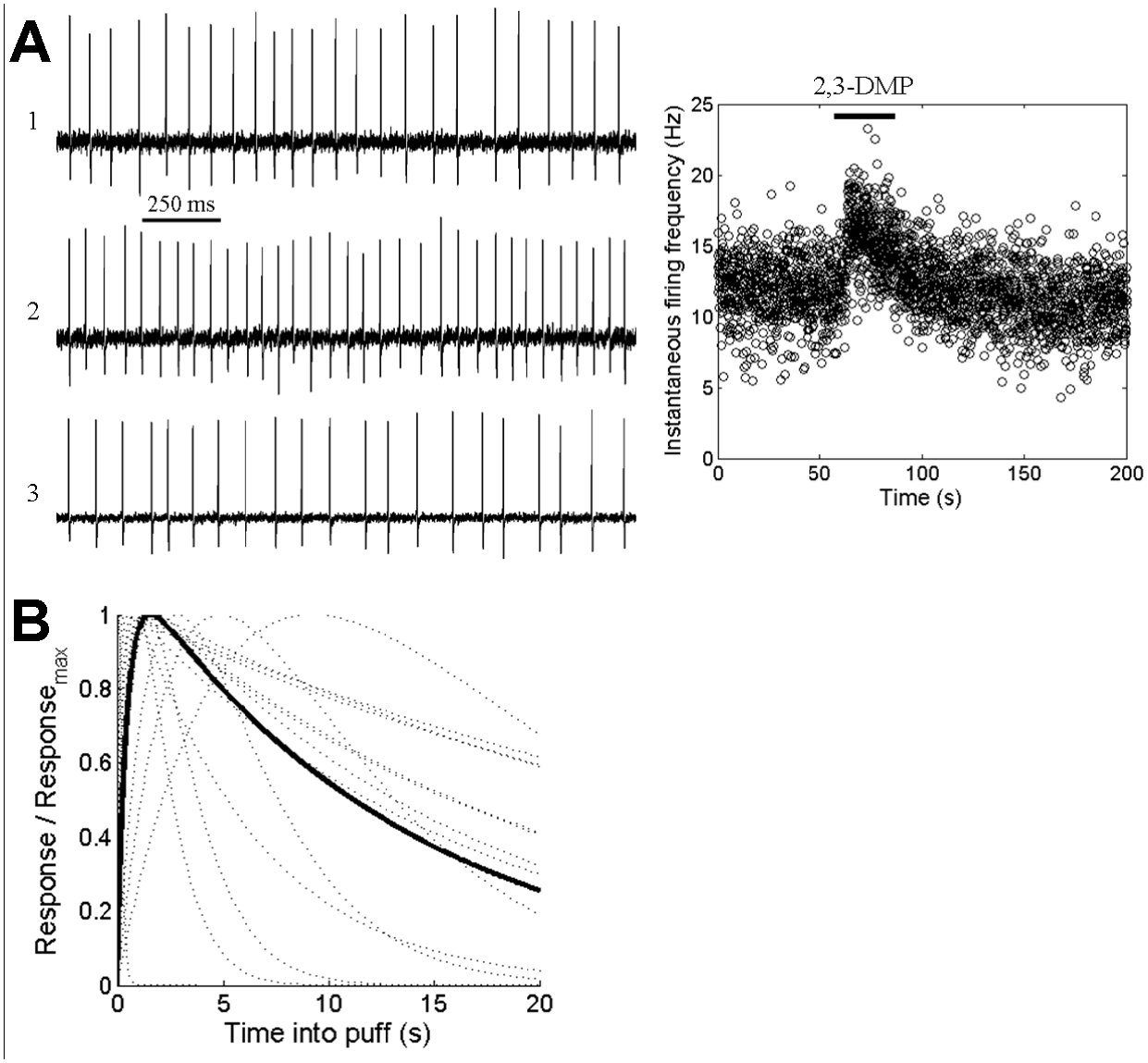

GG neurons in neonatal mice detect 2,3-DMP. A) An RSS-firing GG neuron (left panel) puffed with 9.3 2,3-DMP exhibits an increase in firing rate during (region 2) the puff, relative to before (region 1) and after (region 3) the puff. The frequency vs. time plot (right panel) demonstrates the reversible increase in firing rate. B) Responses to 2,3-DMP exhibited desensitization during a 20 s puff. The median line is shown in black; individual responses over the tested population are dotted gray.

Supplementary Figure 2:

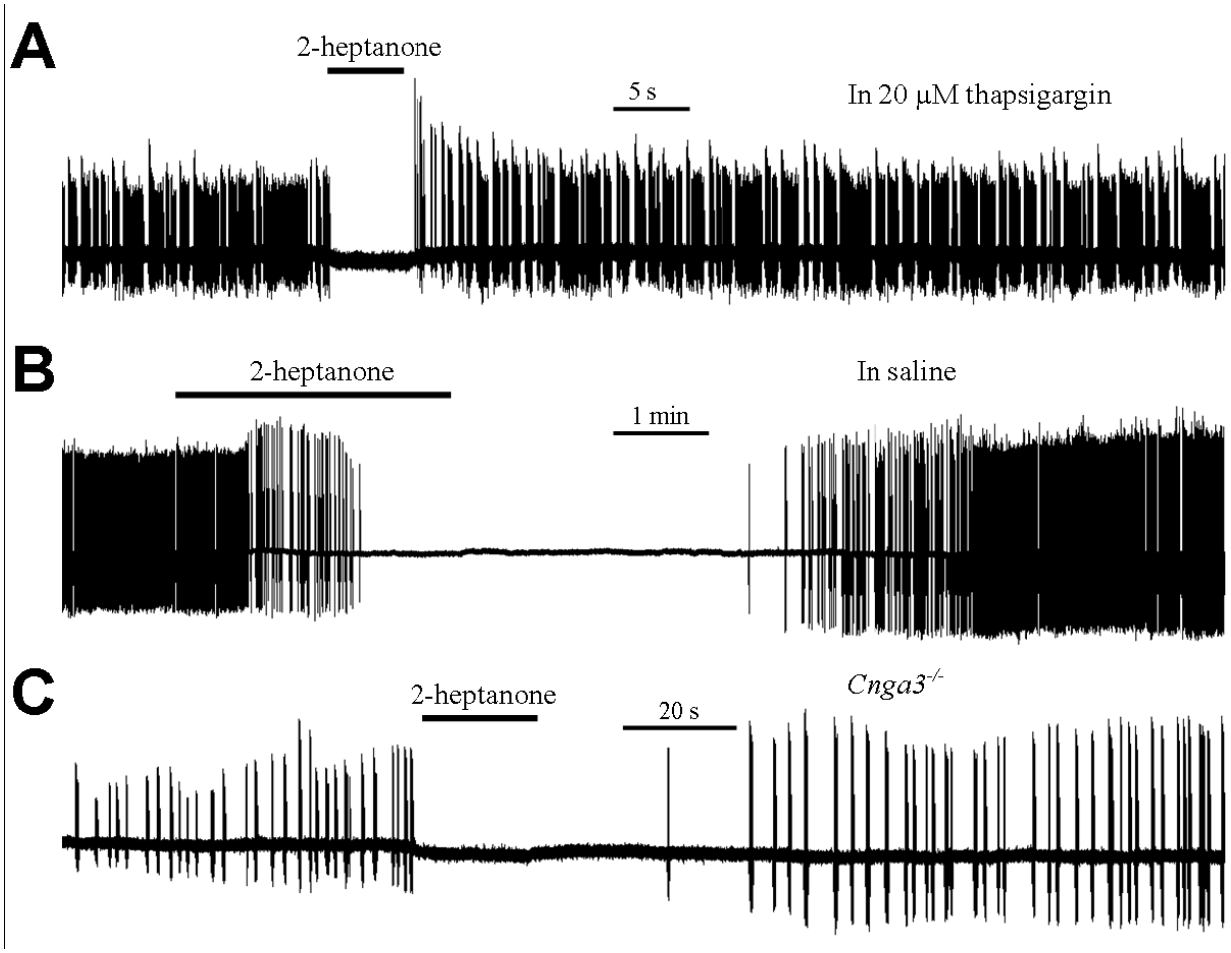

Transduction properties of 2-heptanone. A) Inhibitory responses to 7.2 mM 2-heptanone persisted when GG neurons were pretreated with 20 μM thapsigargin for 30 min. B) Superfusion of 7.2 mM 2-heptanone resulted a sustained inhibition of firing over 5 min. C) Silencing of a GG neuron by 7.2 mM 2-heptanone in a *Cnga3*$^{-/-}$ mouse. Horizontal black bars indicate onset and duration of puffs.

Supplementary Figure 3:

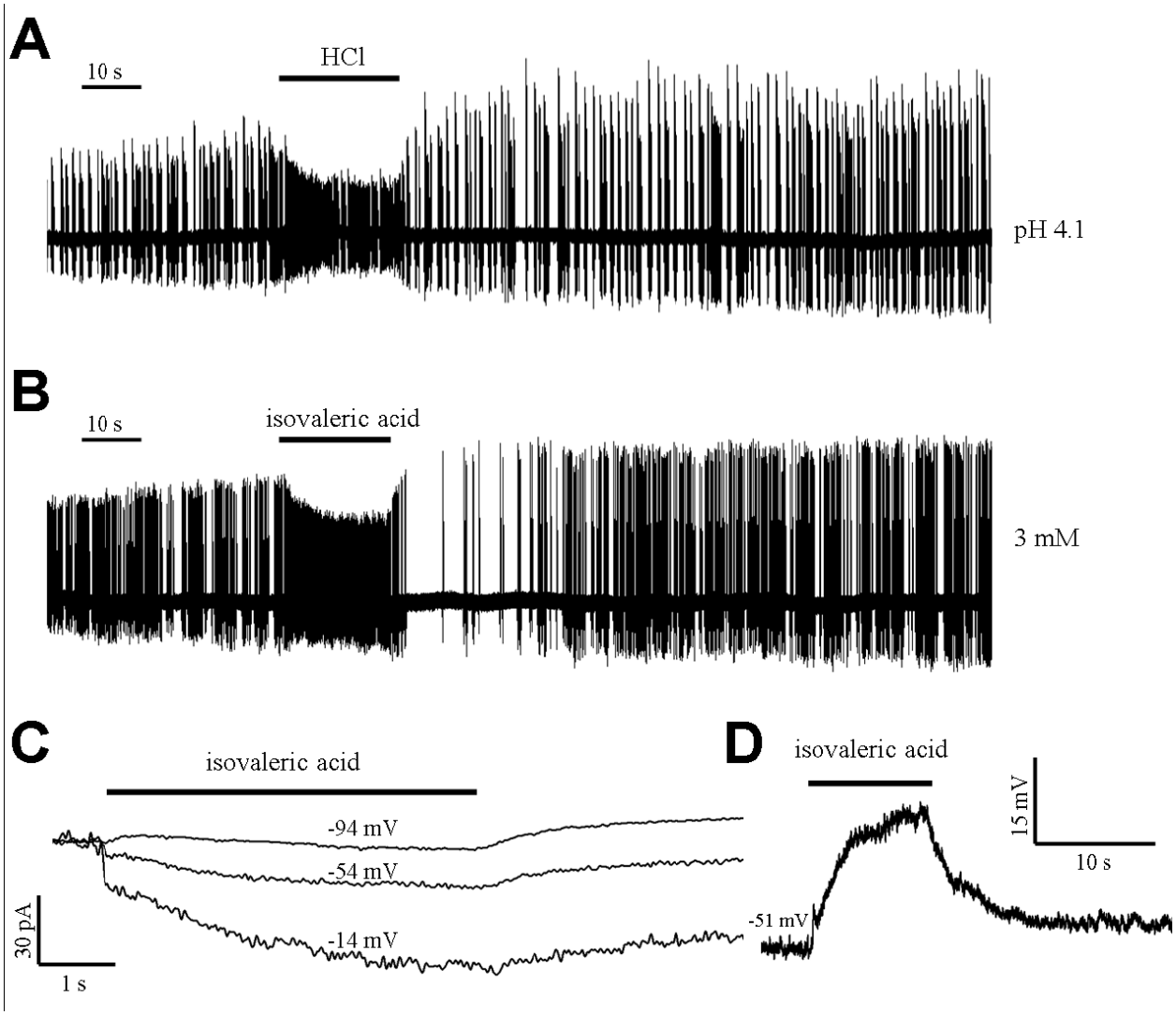

Acidified HBS evokes responses in GG neurons. A) 20 s puff of acidified HBS (pH 4.1 with HCl) excited GG neuron. B) 3 mM isovaleric acid, which acidified HBS to pH 4 also induced neuronal exaltation. C) In whole-cell recordings, puffs of 9.1 mM isovaleric acid at different holding potentials produced an unusual I-V relationship in which inward currents reversed near -80 mV. This is likely due to the shunting of a K^+ conductance. Currents are shown on the same baseline. D) Puffs of 9.1 mM isovaleric acid reversibly depolarized the resting potential of GG neurons.

Supplementary Figure 4:

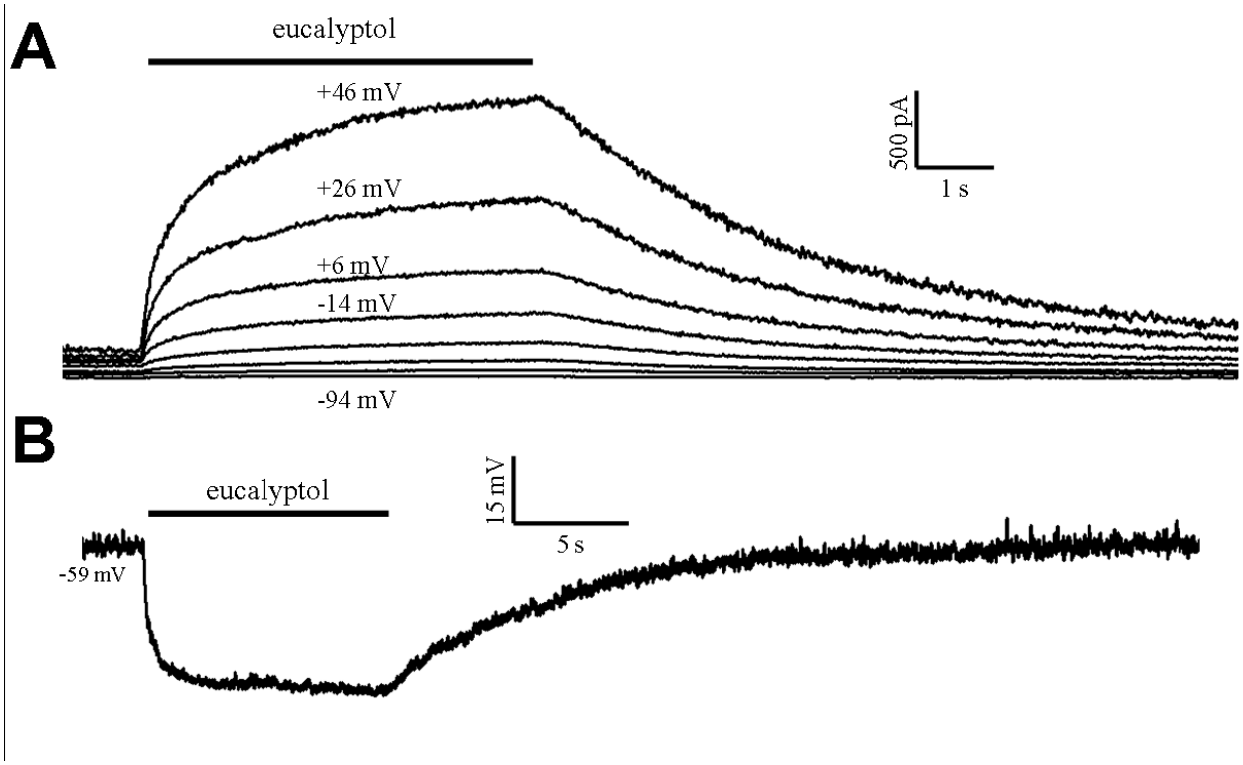

Membrane currents induced by eucalyptol. A) In whole-cell recordings, puffs of 6 mM eucalyptol at various holding potentials induced outward currents similar to those elicited by 2-heptanone. B) Inhibitory effect of eucalyptol is explained by a hyperpolarization of membrane potential. Horizontal black bars indicate time of puff onset and duration.

Supplementary Figure 5:

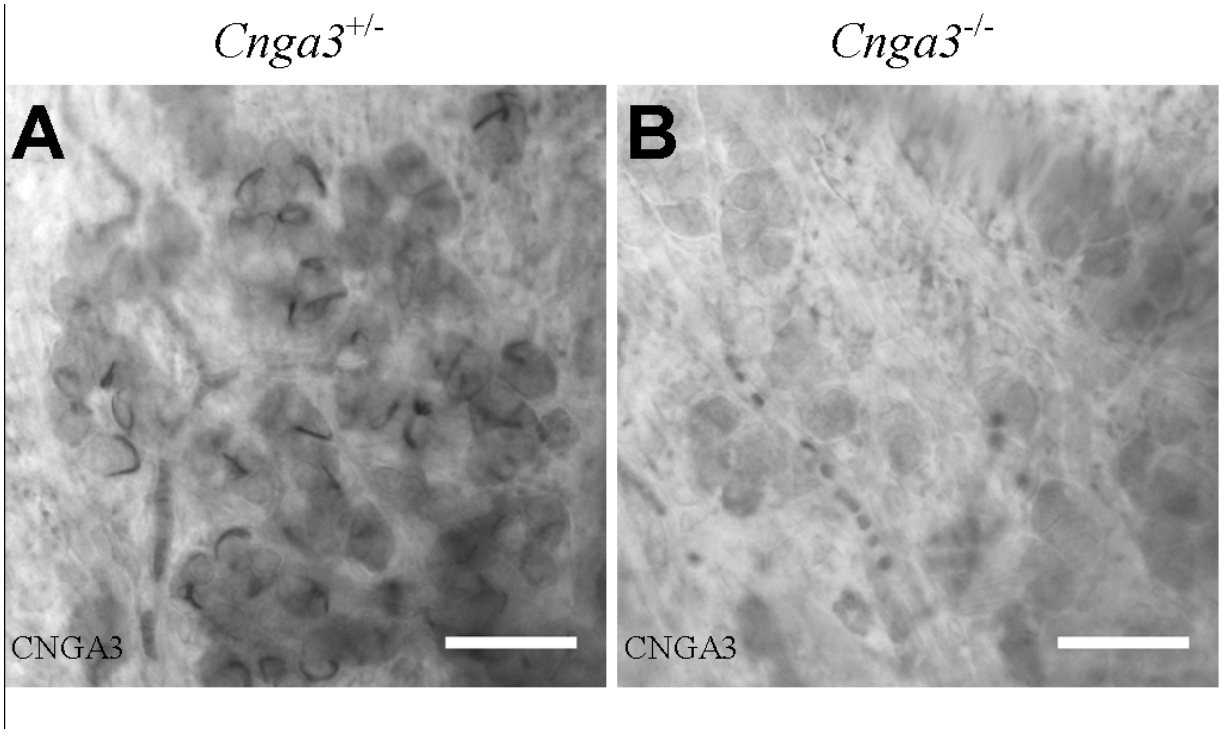

Nominal *Cnga3*$^{-/-}$ mice do not express CNGA3. A specific antibody to CNGA3 labels whip-like subcellular structures on GG neurons of *Cnga3*$^{+/-}$ mice. The labeling is absent in *Cnga3*$^{-/-}$ mice. Scale bars: 40 μm.

Supplementary Figure 6:

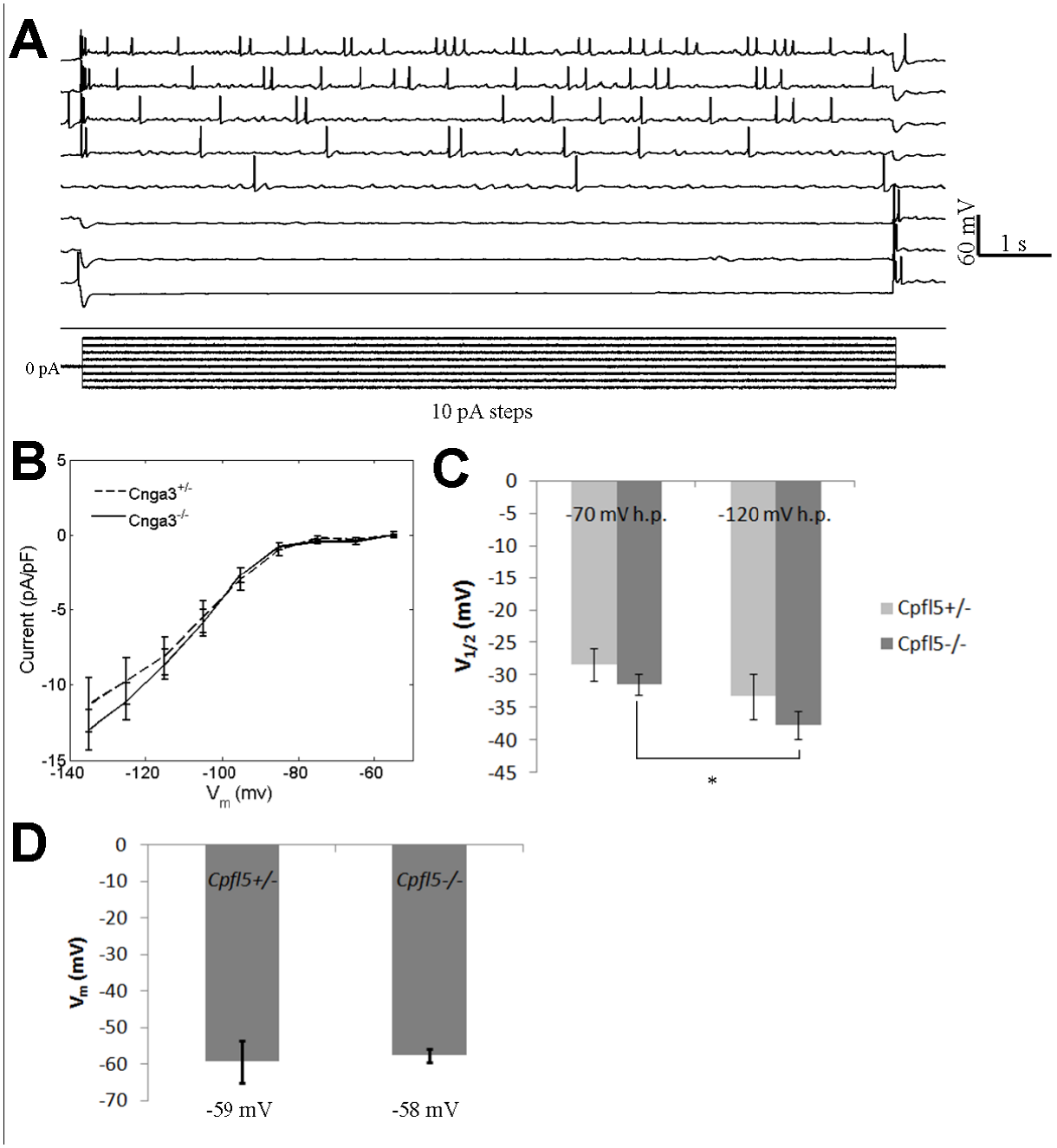

Cnga3$^{+/-}$ and *Cnga3*$^{-/-}$ mice have similar intrinsic membrane properties. A) Shown are data from a *Cnga3*$^{-/-}$ mouse. In whole-cell recordings, 10 s injections of depolarizing current in 10 pA steps from resting potential revealed increase in total spontaneous firing frequency associated with successively larger current magnitudes. Injections of hyperpolarizing current induced sags in membrane potential. These sags are indicative of I_h. Anode-break excitation is also observed. B-D) There was no difference in steady-state

properties of B) I_h, C) Na^+ current activation $V_{1/2}$ values evaluated by voltage jumps from -70 mV and -120 mV holding potentials (h.p.), or D) resting potentials in *Cnga3*$^{+/-}$ vs. *Cnga3*$^{-/-}$ mice. Asterisk (*) indicates statistical significance at $p < 0.05$ (two-sample t-test).

Supplementary Figure 7:

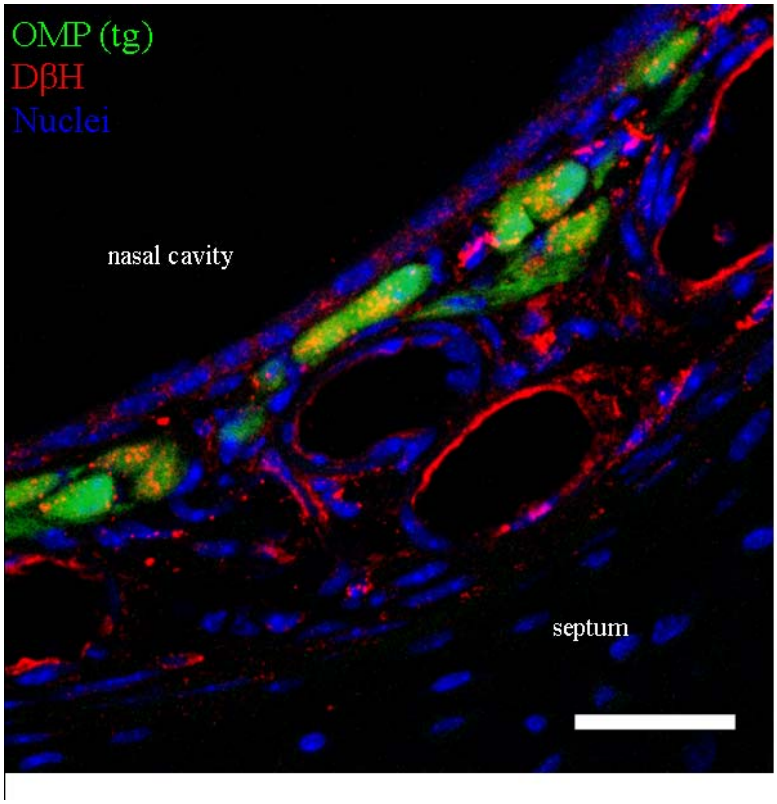

Localization of dopamine β-hydroxylase (DβH) in the nasal vestibule. Shown is the distribution of immunoreactivity for DβH in GG neurons (green) and blood vessel walls. DβH is essential for production of norepinephrine and is a marker of sympathetic nerve varicosities. Scale bar: 30 µm.

Supplementary Figure 8:

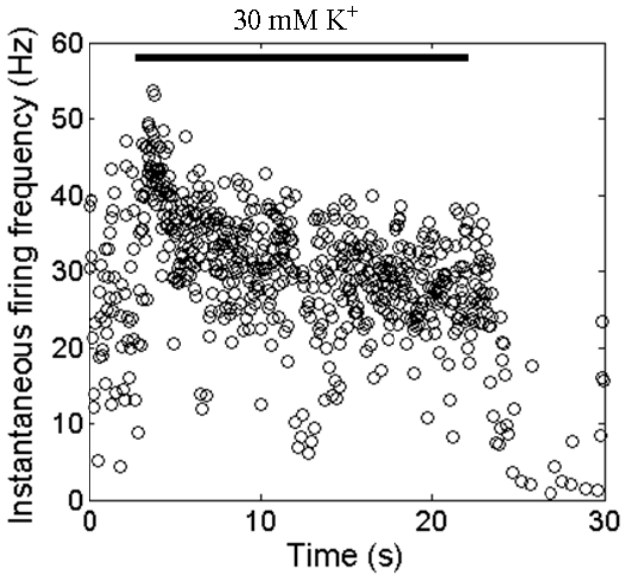

Effect of puffing a hyperkalemic solution. In contrast to responses induced by serum, which were gradually activating, responses induced by a 20 s puff of 30 mM KCl reached maximum within 2 s. Shown is a frequency vs. time plot, with horizontal black bar indicating puff onset and duration.